UNIVERSITY OF NAPLES FEDERICO II

School of Polytechnic and Basis Sciences

Department of Chemical, Materials and Industrial Production Engineering

XXXIV° Ph.D. Programme in
Industrial Products and Processes Engineering

Ph.D. Thesis

On the Braiding Manufacturing of Natural Fibers Composites

Ph.D Course Coordinator
Ch.mo Prof. Andrea D'Anna

Ph.D. Supervisor
Ch.mo Prof. Antonio Langella

Ph.D. Student
Davide Mocerino

Academic Year 2020/2021

Contents

List of Figures

List of Tables

Abstract

This thesis work focuses on the realisation process of braided preforms using hemp fibres. The work can be subdivided into three parts:

Section I: Literature review

Section II: Comparison of different analytical processes to calculate the value of Cover Factor and developing of a new approach to obtain it.

Section III: Mechanical properties of braided hemp preforms.

The braiding technique was used to obtain 2D biaxial and triaxial preforms, with a forecasting approach towards the production parameters and the development of a specific tool for it. With the analytical approach developed in the past, it's clear that, especially in the triaxial preforms, there will be some error in the final calculation of Cover Factor, so it has been necessary to find a unique approach that is valid for all the produced cases.

The use of the statistical approach, in this case, permits to obtain a value of predicted Cover Factor and consequently of the volumetric percentage of fibres that is really close to the wanted one. This thesis project established a valid method to compare the value of the Cover Factor obtained with the statistical approach and the one obtained in the experimental production.

The last part of this work focuses on the study of the mechanical properties of the hemp braided composites, the influence of the value of braiding angle, and the comparison between biaxial and triaxial braided preform with the same Cover Factor that corresponds to the same fibres volume fraction.

Section I

Chapter 1

State of Art

The necessity to produce composite materials with high performances comes from the requirement of large industries such as aerospace or automotive. To afford these requests, advanced textile composites were developed. The typologies of textile composites are classified in this way:

- Woven preform

- Non-Woven preform

- Knitted preform

- Braided preform

Braided composite materials are different compared to the classical composite materials. They have an interlaced structure, and the realization of this kind of composites is totally automated. The production method of braided preforms permits to obtain a tubular composite artefact with a high production rate and mostly with continuous fibres [1]. The braiding process is a technique used since ancient times for making ropes [2],and in the XX century this process was automated to obtain products in the textile industry, such as shoelaces and objects with complex shapes (Figure 1.1)

Figure 1.1: Example of braided products

In the last fifty years, the braided reinforced preforms have been used to create plastic-based composites to obtain a final product that is lighter than metals but is equally strong [3].

The braiding process can be, in fact, used with different kinds of fibres -such as glass fibres, carbon fibres and natural fibres - and with the aim to produce air ducts, fuel lines, turbine blades and reinforced automotive shafts [4].

Indeed, with this production technique is possible to realise holes in the final preform without interrupting the production or without breaking the fibres, avoiding in this way the reduction of mechanical properties [4, 5, 6]. Another advantage is the flexibility that allows to change the shape during the realisation, to obtain bifurcations or section variations.

Braiding composites are made of fibres interlaced diagonally with respect to an axis and, thanks to this structure, they will result more resistant than traditional laminates; as consequence, they will have less stiffness due to the crimp angle [6].

Braiding process can be subdivided in two typologies:

- 2D Braiding (with yarns interlaced only in the plane)

- 3D Braiding (the yarns are interlaced also in the thickness) [1, 7]

The 3D Braiding process has limited use since the size of the preforms is small; this is due to the size of the machines, the high costs of production and the small production rate [8]. Differently, the 2D Braiding process is of major interest from a scientific point of view, due to the possibility to obtain different final manufactures with different shapes (planar, circular, complex shape).

In Table 1.1 there is a comparison between braided 2D and braided 3D technology [9, 10]

Table 1.1: Comparison between different braiding technology

Kind of Preform	Pro	Cons
2D Braided	- Good properties in axial direction - Automatized production process - Good for complex geometry - Good drapability	- Small machine's dimension - Bad properties out of plane
3D Braided	- Good properties in and out of plane - Good for complex geometries	- Slow production process - Small machine's dimension

1.1 History of Braiding Production

A mechanism that permits to move coils with a circular movement around a mobile spindle and permit to obtain an interlaced fabric is called braiding machine.
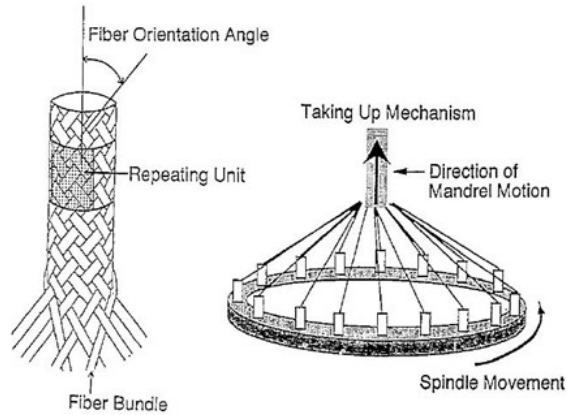
Figure 1.2: Tubular braiding machine

The first braiding machine was developed in the 18th century and before, this kind of production was totally manual. During the past century there was a significant development of these machines due to the study of the process with a cinematic point of view.

A braided preform is determined by three particular fields: the geometry of the fabrics, the design of the final structures (mechanical properties etc.), the development of braiding machines.

Before the existence of the automated braiding process, the axial symmetrical components were realized with the filament winding technology (Figure 1.3)). This technology is optimal to produce straight and short tubes, but to obtain more complex shapes there are many issues, including the costs and the impossibility to have outstanding mechanical properties.
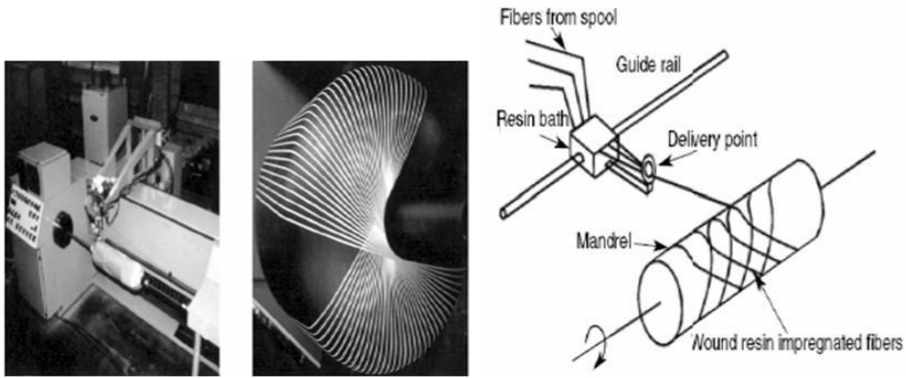
Figure 1.3: Filament winding

Below it is possible to see a list of the advantages of using braiding rather than filament winding [11]:

- Braided preforms have a better fatigue resistance compared to the ones realized with the filament winding process;

- It is possible to use a wide variety of angles and add filaments parallel to the axis of the mandrel;

- It is possible to obtain a wide range of dimensions and complex shapes, not only limited to the circular one;

- The preform obtained with a braiding process can have holes and branches without the need of others working processes, keeping in this way the continuity of the fibers.

- The automation of the process is better than the filament winding, resulting in a higher production rate.

Different studies demonstrated that braiding price is half of filament winding process one because it is faster and easier [12]. Drechsler [13] defined braiding as the best technique in each industrial sector to produce composite fabrics in a cheap way and with high production rates.

Summarizing, a braiding product is composed of unidirectional fibres that are joined in yarns, and each yarn is interlaced with another one composed by fibres in another direction. The angle that the fibres realize with the local axes of the braid is called braiding angle and is one of the most important parameters that shows how the braiding machine has to work [14, 15]. Sometimes is possible to put yarns in longitudinal direction so to give an improvement to the longitudinal properties of the preforms [16].

The ideal geometry of the braid is when yarns are equally spaced and there is a repetition of the geometry. This geometry, called pattern, could be of three different typologies (Figure 1.4): diamond braid (one-over-one overlap), regular braid (one-over-two overlap) and Hercules braid (one-over three overlap) [16].

Figure 1.4: Braiding Pattern: a) diamond, b) regular, c) Hercules

The mechanical properties of a braided preform are influenced by the pattern and by the orientation of yarns. In Figure 1.5 is possible to see how different the patterns and respective yarns undulation are [17]. Different braiding architectures influence the mechanical performances of the final composites, and this linkage is a foundamental point for different studies from different authors like Wolfahrt [18] and Ifju [19].
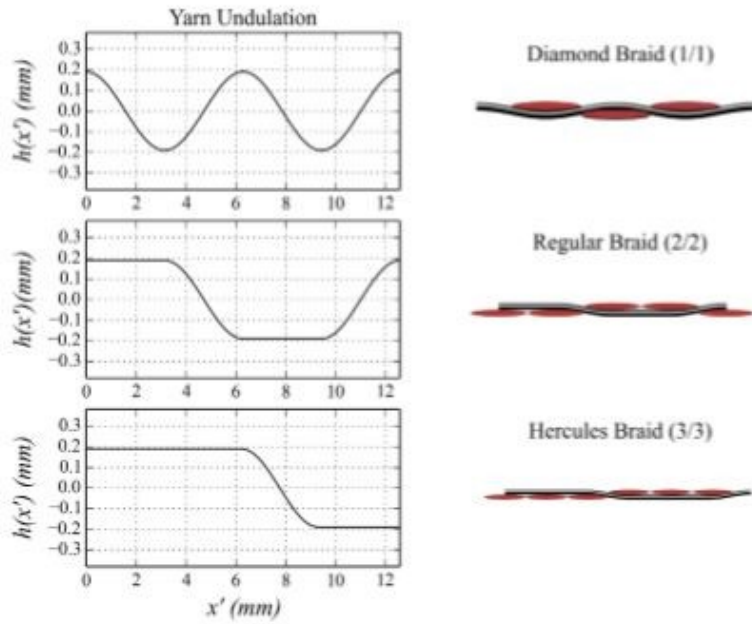
Figure 1.5: Comparison between different kinds of braiding patterns

In Figure 1.6 it is possible to observe different types of braided preforms obtained with different production processes [20].

Other kinds of preforms, like rectangular bar or bar with I,T,C shape, can be obtained with this process [11]. Indeed, different shapes of the mandrel permit to obtain different braided preforms [21].

Braid preform shape	Production process
Tubular	• 2-D maypole biaxial with mandrel • 2-D maypole triaxial with mandrel • 3-D tubular with mandrel
Diamond braid	• 2-D maypole biaxial Fig. 3.1(a)
Regular braid	• 2-D maypole biaxial Fig. 3.1(b)
Hercules braid	• 2-D maypole biaxial Fig. 3.1(c)
Diamond braid with longitudinal reinforcement (triaxial)	• 2-D maypole biaxial
Regular braid with longitudinal reinforcement (triaxial)	• 2-D maypole biaxial
Hercules braid with longitudinal reinforcement (triaxial)	• 2-D maypole biaxial
Flat	• Jacard braider that has a track that loops back
Overwrapped tubular	• 2-D maypole biaxial with inner core of bundled yarns • 2-D maypole triaxial with mandrel with inner core of bundled yarns
H-Beam	• 3-D rotary braiding machine • Track 3-D braider
I-Beam	• 3-D rotary braiding machine • Track 3-D braider
T-beam	• 3-D Cartesian • Track 3-D braider
C-Beams	• 3-D Cartesian • Track 3-D braider
Rectangular Beam	• 3-D Cartesian • Track 3-D braider
Triangular Beam	• 2-D maypole biaxial with mandrel • 2-D maypole triaxial with mandrel • 3-D tubular
Channel Beam	• 2-D maypole biaxial • 2-D maypole triaxial • 3-D tubular
Angle Beam	• 2-D maypole biaxial with die (braidtrusion) • 3-D rotary braiding machine
Square braids and solid column	• 3-D Cartesian • Track 3-D braider

Figure 1.6: Braid Preforms and Braiding production process [20]

1.2 Types of Braiding machines

The braiding machines are divided into two big groups: horizontal machines and vertical machines [20]; the difference lies in the preform production direction. A deeper analysis brings to another classification:

- *Maypole braider machines*, that are used for the production of braided rope and for the braiding production with simple and complex mandrels [22]

- *Flat braider machine*, in which the carriers don't make a complete circular movement.

- *Rotary braiding machines*, in which the carriers don't have a sinusoidal movement [17]. In these machines, there are two sets of coils, the inner and the outer coils, that rotate on two opposite circular paths.

- *Circular braiding machines*, which reduce the variation of tension on the yarns during the production, so to reduce the damage on these elements [2].

The most common methods to realize braided preforms are Rotary Mechanism Procedure [23] for 3D preforms and the Circular Braid Machine [24, 25] specialized in 2D preforms. Other types of braiding machines can be found in literature [5, 26].

The Rotary Mechanism Procedure has a rectangular section and the preform is locked on the top of the coils which rotate on a plane. The yarns are positioned with the axis parallel to the axial direction of the mandrel (less common is a machine with the yarn's axis in a different position) and the movement is realized using gear wheels under the coil plane (Figure 1.7).
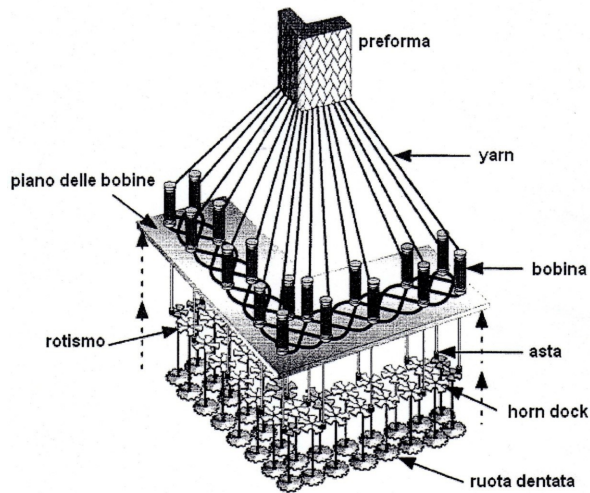
Figure 1.7: Rotary Mechanism Machine

The Circular Braiding machine is the one used in this study. This machine is subdivided in two zones; in one there is the mandrel, around which the fibres will be placed, in the other part of the machine there are the rotary mechanisms for the coils and to interlace fibres. Usually, one of the two zones is moving (frequently is the mandrel) and the other one is fixed [27] (Figure 1.8); the mobile part could move only in the axial direction with a designed speed (take-up speed).
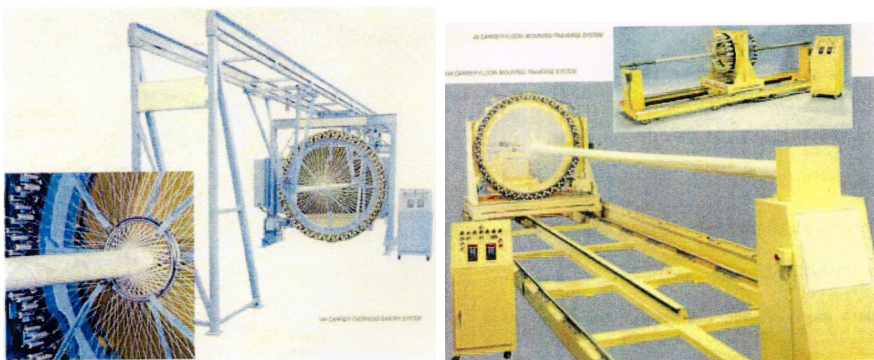
Figure 1.8: Two kinds of Circular Braiding Machine. On the left the mandrel is moving, on the right is the machine to move on a fixed mandrel.

In Figure 1.9 it can be seen how a circular braiding machine works with all the parts that participate in the production of the preforms.
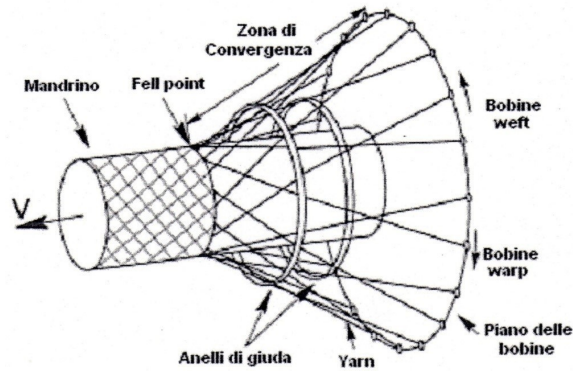
Figure 1.9: Schematic Circular Braiding Production

Regarding fibres, half of the coils has a clockwise rotation (warp) and generate warp yarns of braided preform, the other half (weft) has counterclockwise rotation in the same plane, generating weft yarns [28]. The angular velocity $\pm\omega_h$ on a sinusoidal path, around the mandrel, is the same for all the coils (Figure 1.10).
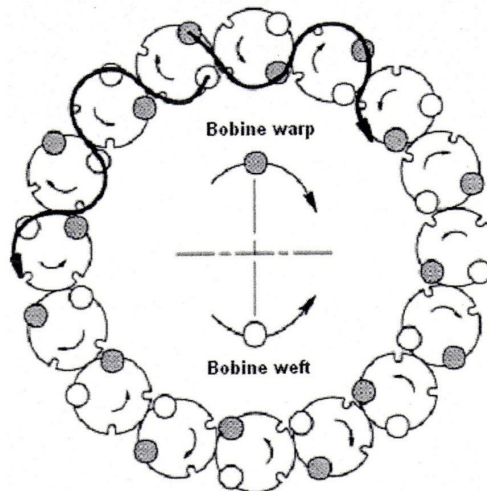
Figure 1.10: Movement of the coils on the sinusoidal path

The interlaced yarns realize a biaxial fabric on the mandrel. Particular machines permit to put a third group of yarns in the longitudinal direction so to obtain a triaxial preform and a better resistance of the final parts in that direction [29] (Figure 1.11).
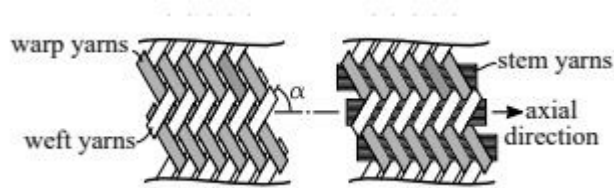
Figure 1.11: Biaxial braid on the left figure and triaxial braid on the right one

Normally, a radial braiding machine is composed of horn gears (Figure 1.12) that permit the rotation of the coils. They have different numbers of slots in which the coils are pushed around the path [30]. The dimension of the horn gears and the number of slots define the dimension of the pattern of the braid and so the final properties of the preforms.

Other components of the machine are the carriers (Figure 1.13), on which the coils are adapted, and they will move together on the sinusoidal path. This part is important because give the tension to the yarn keeping it constant during all the production process [26].

Figure 1.12: Horn Gears

Figure 1.13: Carriers

In some braiding machines, there is a take-up mechanism that permits to move the mandrel, but the advanced ones work with a robotic arm that can move the spindle on six axes so to product preforms with particular shapes [22].

1.3 Defects of Braided PreForm

Usually, in reality, preforms cannot be realized without the presence of defects inside. The most common are:

- irregular yarns space caused by a low tensile tension on the yarn during the production process

- yarn crimping (curvature of the yarn)

- yarn pushing (non-uniform dimension of yarns due to the pressure caused by the other yarns)

1.3.1 Crimping

Yarns that should be straight, but during the process they will assume an undulate shape. This kind of defect known as *crimping* is generated by the wrong kind of tension of the yarns, and the final product results to have local different thicknesses.
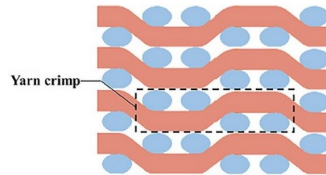
Figure 1.14: Yarn Crimping [31]

1.3.2 Pinching

This kind of defect is common when yarns are not evenly pressed, showing ruffles and variable cross-sections. The defect is called pinching and is due to different reasons: friction between close yarns, wrong tension of wires, jamming of the machine [32].

Modelling the deformed yarns to predict the influence of defects on mechanical properties is a really hard task.
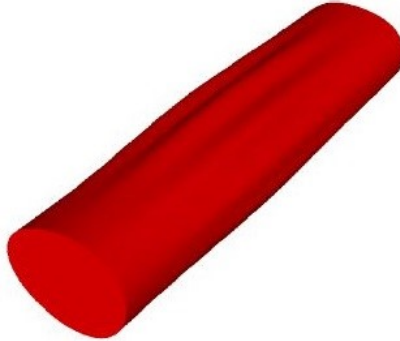
Figure 1.15: Modelling of yarn pinching [32]

1.3.3 Non-Uniform yarn spacing

Due to the low tension of yarns or to the friction between them, it is really hard to obtain an uniform yarns spacing, consequently it is not easy to obtain perfect unitary cells from a geometrical point of view. As a consequence of this defect, the result will be wires that are not straight or parallel and braiding angles different from the designed ones. After the interlacing process, when the preform will be impregnated with an infusion process, the defect will be magnified due to the injection of flux that will move the yarn from the starting position.
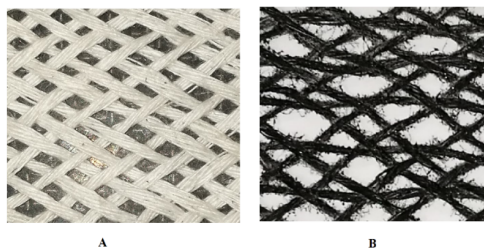
Figure 1.16: Movement of the yarn from the designed position:A biaxial braided preform, B triaxial braided preform

1.4   Application of braided composites

Braiding results to be a competitive technology to realize composites materials. It's useful to obtain tubes and ropes but also for application where high performances are needed. Biomedical and automotive sectors are increasing their production with this process, but the aerospace industry is the one that uses braiding more than the others. The possibility to obtain different shapes with an easy process permits this industry to produce parts of the plane like fuselage or mobile components [33].

Figure 1.17: Example of products realized with Braiding reinforce. On the left there are aircraft windows [7], on the right engine blades

1.5 Analitycal study of 2D Braided pre-form

1.5.1 Yarn Geometry

The braided geometry is defined by the mandrel geometry, but there is more than one parameter that must be taken in consideration. An important element to describe a braided preform is the yarn, a group of fibres that will be interlaced with another one during the production process. When the yarn is placed on the mandrel it will be deformed, consequently, the yarn cross-section could be an ellipse, a circle or a segment, depending on the tension applied on it and from the kind of material that is used. The number of the fibres inside a yarn is called *"filament count"* (nk)
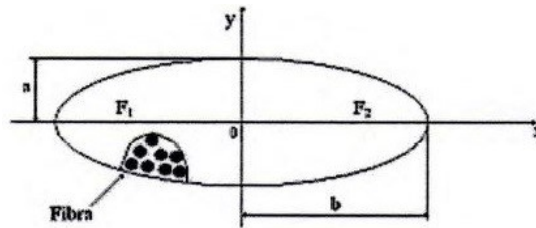
Figure 1.18: Deformed yarn

In Figure 1.18 it is possible to see the semi-major axis of the ellipse *"b"* and the minor one *"a"*. Doubling the first one the width of the yarn *"W_y"* is obtained, doubling the second one the height of the yarn **"2a"**.

The area of the ellipse is

$$S_B = \pi a b \tag{1.1}$$

The equation 1.1 keeps in consideration the sum of the surface with fibers and with resin. Indeed the fibers could be compressed considerably, but there will be an empty space that will be occupied by the resin. The packing factor F_p describes the space occupied by the fibers (S_f) in relation with the total one.

$$F_p = \frac{S_f}{S_B} \tag{1.2}$$

Considering the hypothesis that the packing factor is constant and not depending from cross section of the yarns, it is possible to imagine that the fibers are placed side by side so to have a rectangular cross section
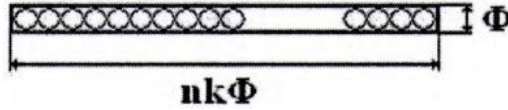
Figure 1.19: Theoretical cross section

with this configuration the rectangular cross section will be:

$$S_B = nk\Phi\Phi = nk\Phi^2 \tag{1.3}$$

with Φ diameter of fiber.

The area occupied by the fibers will be

$$S_f = nk\pi \left(\frac{\Phi}{2}\right)^2 = nk\pi \frac{\Phi^2}{4} = \frac{\pi}{4}(nk)\Phi^2 \tag{1.4}$$

Knowing S_B and S_f it is easy to obtain the packing factor F_p:

$$F_p = \frac{S_f}{S_B} = \frac{\pi(nk)\Phi^2}{4(nk)\Phi^2} = \frac{\pi}{4} = 0.785 \tag{1.5}$$

It can be noticed that the packing factor is independent by the single fiber, by the number of fibers into a yarn and by the disposition of the fibers in a yarn.

It is also possible to obtain a relation between the height and the width of the yarn:

$$a = \frac{S_B}{\pi b} \tag{1.6}$$

Doubling both the members of the equation and substituting equation 1.5 in the equation, it will be possible to obtain:

$$2a = \frac{2S_B}{\pi b} = \frac{2S_f}{\pi b F_p} = \frac{2nk\pi\Phi^2}{4\pi b}\frac{1}{F_p} = \frac{nk\Phi^2}{2b}\frac{1}{F_p} = \frac{nk\Phi^2}{W_y}\frac{1}{F_p} \tag{1.7}$$

Giving nk and Φ and knowing F_p that has a constant value of 0.785 it is possible to calculate the dimension of the cross section of yarns. Usually, W_y could be measured with a microscope and consequently the value of the height 2a will be known. The thickness of the braided preform is due to two yarns overlapped; so, considering that all the yarns have the same deformation, the thickness will be:

$$t = 22a = 4a = \frac{2nk\phi^2}{W_y}\frac{1}{F_p} \tag{1.8}$$

1.5.2 Geometry of unit cell

The braided preforms are characterized by a repetition of a defined rhomboidal geometry called unit cell. In Figure 1.20 it is possible to see the unit cell with two basic parameters for the production of braided preforms.

The first one is the braiding angle θ_s, defined as the angle between the yarn and the mandrel axis; the second one (h), is the dimension of the unit cell [36].
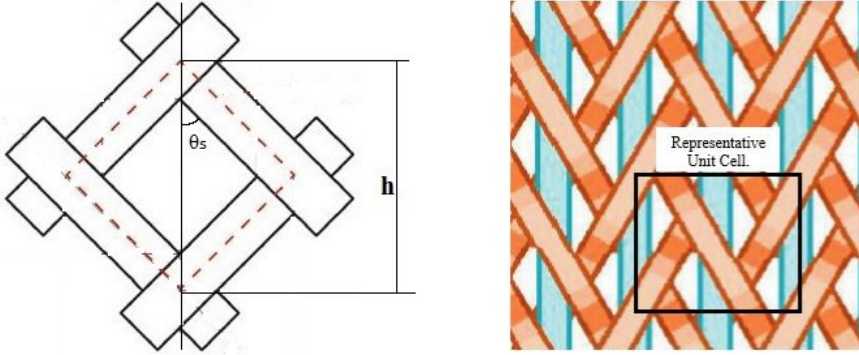
Figure 1.20: Unit cell of braided preform [34] [35]

Brunshweiller [2] was one of the first to describe the braiding geometry considering the unit cell as the smallest repeating unit of the braid. It is necessary to pay attention to the possible changes of shape of the mandrel that could influence the unit cell. In addition, a change of mandrel's axial velocity causes a change in the braiding angle [13]. The 2D preforms are composed of superficial unit cells and these elements are controlled only by the braiding angle and by the production step, that is the length of the preform realized in each coil cycle. Changing the braiding angle θ, the value of the step h changes so that the quantity L_B (the distance between two parallel yarns) is held constant (Figure 1.21).
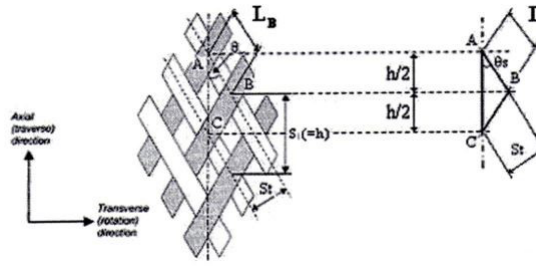
Figure 1.21: Geometry of 2D braiding

From Figure 1.21 it is easy to calculate from a geometrical point of view the following equations:

$$L_B = \frac{h}{2} \frac{1}{cos(\theta)} \qquad (1.9)$$

$$\frac{S_t}{2\sin(\theta)} = \frac{h}{2} \qquad (1.10)$$

with L_B corresponding to the distance between two overlapped fibres.

Replacing $\frac{h}{2}$, calculated in the equation 1.9, in 1.10:

$$\frac{S_t}{2\sin(\theta)} = L_B \cos\theta$$

$$S_t = 2L_B \sin(\theta)\cos(\theta) = L_B sin(2\theta) \qquad (1.11)$$

with S_t the distance between two parallel yarns.

Considering the equation 1.11 it is possible to find the minimum value of braiding angle called *"locking angle"* (θ_L). When the braiding angle reaches this value, all the yarns will have the same direction of the mandrel axis and they will touch each other, so the dimension of the unit cell S_t will be equal to the yarn width W_y.

In this case, the 1.11 will become:

$$W_y = L_B \sin 2\theta_L \tag{1.12}$$

and it will be easy to calculate the locking angle

$$\theta_L = \frac{1}{2} \sin^{-1} \left(\frac{W_y}{L_B} \right) \tag{1.13}$$

When the value of braiding angle is lower of this one the yarns start to overlap each others and the machine will be locked. This could happen also for the values of braiding angle that are too big; in this case, the yarn will be overlapped in a circumferential direction. So, the braiding angle θ has to be in the range:

$$\theta_L \leq \theta \leq 90 - \theta_L$$

Du and Popper [27] defined another analytical way to calculate the locking angle:

$$\cos(\theta_L) = \frac{W_y \sin(\gamma)}{2 R_m \sin(\frac{2\pi \sin \gamma}{N_c})} \tag{1.14}$$

were W_y indicates the yarn thickness, N_c indicates the number of yarn support, R_m is the mandrel radius and γ the half of the cone angle of the mandrel.

1.5.3 Cover Factor

The **Cover Factor** is an important parameter in the production of braided preforms. It represents the mandrel area covered by the preform linked with the total mandrel area, and it is also an information of the preform density. At first analysis, it is easier to calculate the cover factor referring to the single unit cell [11], but it is important to highlight that this parameter is referred to the entire preform.

1.5.3.1 Influence of different parameters on the cover factor

The major influence on the value of the cover factor comes from the value of braiding angle θ: generally keeping constant other variables, the cover factor will increase with the increasing of the braiding angle.

A different thing happens when the value of mandrel Radius is considered: indeed, increasing the Radius, the Cover Factor will decrease.

A third influence is the number of coils; it is clear that with increasing N_c there are more filaments and consequently a bigger cover factor. The same can be said considering the width of the yarn.

In a real situation it is not easy to predict the cover factor, because all the parameters are not fixed and so they interact each other influencing the final covering of the mandrel. Melenka [20] tried to graph the relationship between different variables during the production process. (Figure 1.22, Figure 1.23 and Figure 1.24)
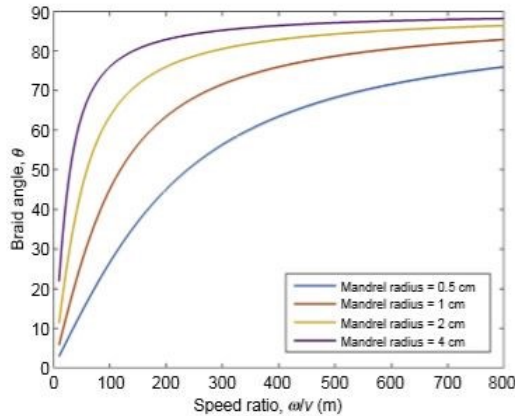
Figure 1.22: Braiding angle and the ration between angular velocity of horn gear and take off velocity of the mandrel changing the dimension of this last one
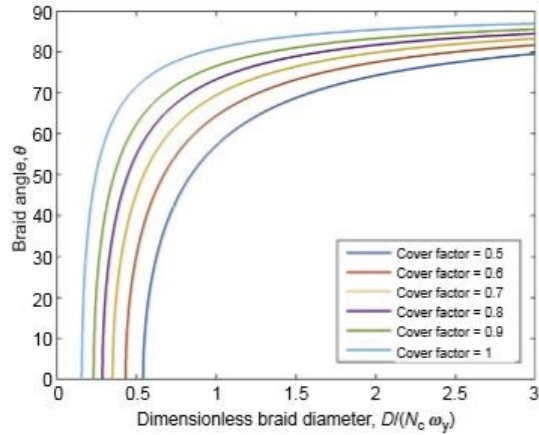
Figure 1.23: Braiding angle linked to a non-dimensional value of diameter for different value of cover factor.
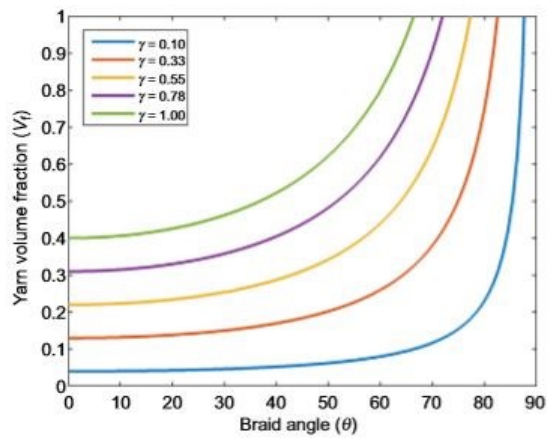
Figure 1.24: Braiding angle linked with fiber volume fraction for different value of the angle between the guide and deposition plane.

1.6 Application to a Radial Braiding Machine

1.6.1 Process Parameters

There are some parameters that describe the way a radial braiding machine works:

- $\boldsymbol{N_c}$: total number of coils applied on the horn gears, an half is clockwise and the other one is counterclockwise.

- **R [mm]**: mandrel radius; sometimes it is possible to use the mandrel diameter D_m.

- $\boldsymbol{\omega}$ **[rad/s]**: angular velocity of coils around the mandrel axis

- **v [mm/s]**: translation velocity of mandrel, indicated also as "*take up speed*".

Other important parameters are the *"Ley Length"* [LL] and the *"Horn Gear Speed"* [HGS], which are the only two values to control the machine used in this study.

Ley Length

The quantity of textile that is wrapped around the mandrel axis during one turn of the coil around the center of the machine is called lay length [mm]. It can be seen in Figure 1.25

The base of triangle is the circumference of mandrel, consequently:

$$LL = 2\pi R \cot(\theta) \tag{1.15}$$
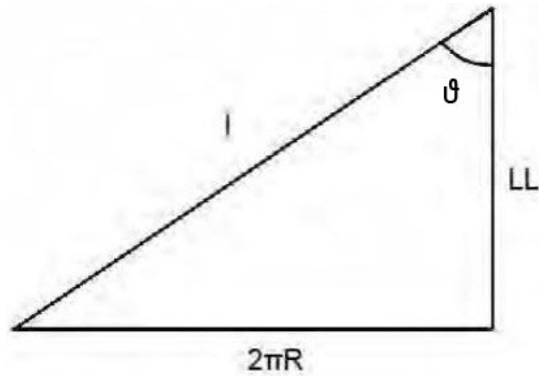
Figure 1.25: Lay Length scheme

With equation 1.15 it is possible to obtain a relationship between a process parameter (LL) and a geometrical one (θ). So, fixing the desired value of braiding angle and the desired mandrel radius, there is only one value of lay length.

Horngear speed

The velocity of horngear around their axis is called horn gear speed (HGS) [round/min] and it influences the velocity of the coil around the axis of the mandrel, and therefore production rate of textile (*"linear production rate [mm/s]"*). This parameter doesn't affect the geometric characteristics of the preform.

1.6.2 Braiding cinematic

During the production of braided preforms on a circular braiding machine, the yarns follow an helical trajectory with a winding angle equal to the braiding angle. In Figure 1.26 it is possible to see the influence of the mandrel velocity (v) and of the yarn circumferential velocity (ω R) on the trajectory of itself [29].
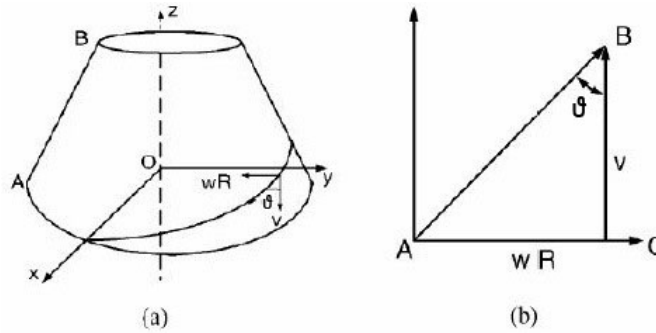
Figure 1.26: (a) yarn winding on the mandrel; (b) velocity vector [11]

From the geometrical figure it is possible to calculate:

$$\theta = \tan^{-1}\left(\frac{\omega R}{v}\right) \tag{1.16}$$

The angular velocity of the horngear (ω_h) can be linked to the angular velocity of the coils around the center of the machine (ω). Indeed, for each horngear rotation, the coil is changed going on another horngear, walking at an angle equal to α (Figure 1.27)
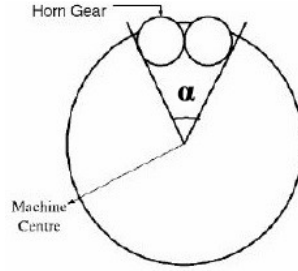
Figure 1.27: Horn gear in the plane

So the angular velocity of the coils will be:

$$\omega = \frac{\alpha}{t} \tag{1.17}$$

with t[s] the time taken by the horngear to rotate

$$t = \frac{2\pi}{\omega_h} \tag{1.18}$$

and α [rad] the angle made by two horngears:

$$\alpha = \frac{2\pi}{\frac{N_h}{2}} = \frac{4\pi}{N_h} \tag{1.19}$$

where N_h is the number of horngears.
Substituting the equations 1.19 and 1.18 in 1.17:

$$\omega = \frac{2\omega_h}{N_h} \tag{1.20}$$

going back to the 1.16, it is possible to obtain the braiding angle in function of the angular velocity of the horngear (ω_h)

$$\theta = \tan^{-1}\left(\frac{2\omega_h R}{N_h v}\right) \tag{1.21}$$

Looking to Figure 1.28, the braiding angle could also be linked to the length of the winding helix L [37]:
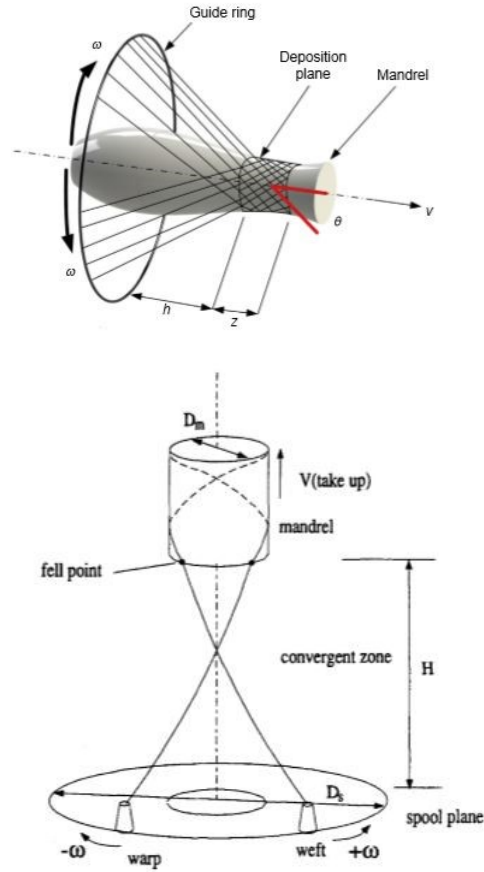
Figure 1.28: Different variables that influence the braided preforms

$$L = \frac{\pi D_m}{\sin(\frac{\theta}{2})} \qquad (1.22)$$

This parameter, if the mandrel diameter is known, could give an indication of the density of the braid.

In Figure 1.28 it is also indicated the position of the deposition plan of the machine relative to the mandrel and it is called convergent zone (H) [27]. This value could be changed with fixtures such as guide rings or using a different technique called reverse braiding [38].

1.7 Aims and Scope

As highlighted in the previous paragraphs, taking into account the importance of the cover factor for the production of braided preforms, it is possible to assess that it is necessary to go deeper into the study of this parameter and it will be crucial to understand what are the factors influencing it. In the next chapter, different ways to calculate this variable will be introduced and a lack of research about the realization of braided preforms using fibres with a particular elastoplastic behaviour will be underlined, especially in the case of triaxial preforms. Different approaches will be shown for the evaluation of the cover factor, each validated on carbon fibres preforms. The final aim of this work is to underline a new analytical/statistical process that permits to obtain good value in terms of Cover Factor and consequently in terms of fibres volume percentage of the final products. The methods presented in the literature to calculate the CF have not shown good matching between the predicted value and the real value of this factor on the produced preforms. This is, on one hand, related to the particular behaviour of the fibres but it is also linked to the lack of knowledge about the full process. It will be clear the difference that will result using the literature approaches on our kind of fibres and the error on the estimation of Cover Factor, indeed the reported classical approach that uses the developed analytical form during the years shows an absence of precision and a considerable mistakes in the calculations, but the new way to consider the unit cells and the disposition of the fibres will permit to forecast in a better way the Cover Factor in the case of fibres with a more plastic behaviour and will cover the lack of knowledge in this field, improving the precision in the manufacturing process of the braided preforms.

Section II

Chapter 2

Evaluation of Cover Factor

2.1   2D Biaxial Braided Preforms

Considering a real braided preform, it is possible to notice that the number of unit cells on the mandrel is equal to the half of the number of coils $(\frac{N_c}{2})$.

In Figure 2.1 it is possible to notice that the sides of the rhombus are equal to the half of the yarn width $\frac{W_y}{2}$. Considering that on the mandrel there are $\frac{N_c}{2}$ unit cells, each one will have a width equal to:

$$AB = \frac{2\pi R}{\frac{N_c}{2}} \tag{2.1}$$

It is possible from the geometry to calculate the height of the triangle ABC in Figure 2.1, so its area will be:

$$A_{ABC} = \frac{1}{2}\left(\frac{4\pi R}{N_c}\right)\left(\frac{4\pi R}{2N_c \tan\theta}\right) = \frac{4\pi^2 R^2}{N_c^2 \tan\theta} \tag{2.2}$$

ABC is the half of elementary cell.
Consequently it is clear that the value of BB' A'B' are:

$$BB' = \frac{W_y}{2\cos\theta} \tag{2.3}$$
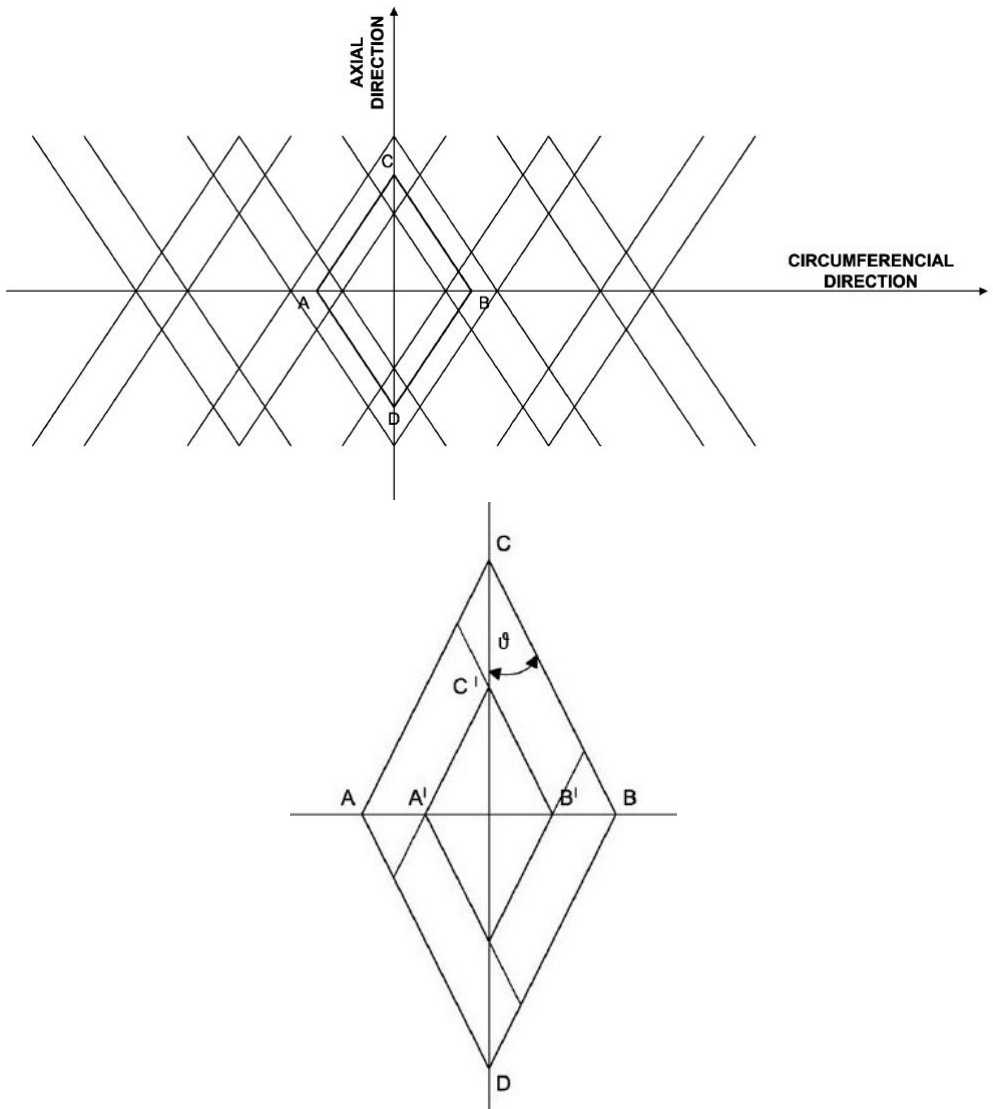
Figure 2.1: Arrangement of unit cells on the mandrel and unit cell used for the calculation of cover factor

$$A'B' = AB - AA' - BB' = AB - 2BB' = \frac{4\pi R}{N_c} - 2\frac{W_y}{2\cos\theta} \qquad (2.4)$$

From the geometry it is possible to obtain the height of A'B'C' and consequently the area of that triangle:

$$A_{A'B'C'} = \frac{1}{2}\left(\frac{4\pi R}{N_c} - 2\frac{W_y}{2\cos\theta}\right)\left(\frac{4\pi R}{N_c} - 2\frac{W_y}{2\cos\theta}\right)\frac{1}{2\tan\theta} \qquad (2.5)$$

A'B'C' results to be the half of the area of the unit cell without fibers. Since the unit cell is symmetric to the segment AB, the value of cover factor can be considered equal to the one of the full cell.
At this point it is possible to calculate the cover factor considering the following equation [11]:

$$CF = 1 - \frac{A_{A'B'C'}}{A_{ABC}} = 1 - \left(1 - \frac{W_y N_c}{4\pi R\cos\theta}\right)^2 \qquad (2.6)$$

Talking about mechanical resistance of the final product, it is important to know another variable: the fiber volume fraction [39]; this parameter is dependent by the unit cell geometry and by the shape of the yarn that could be obtained making some microscope analysis [40]. Starting from the knowledge of the cover factor, it is possible to use the following equation to link the fibres volume fraction with the other production parameters.

$$V_f = \frac{W_f N_c}{4\pi R_0 \cos\theta} \qquad (2.7)$$

As seen before, this analytical approach is valid for circular mandrels, or asymmetric mandrels, replacing in the equations the terms of the radius of the mandrel with something linked to the perimeter of the new one. The important thing is to consider a constant braiding angle during all the production process [24].

2.1.1 Percentage of Overlap

The cover factor equation doesn't consider the possibility of overlapped yarns. As said, this could happen if the braiding angle is too big or too small. For this reason, it is necessary to define a way to calculate the maximum admissible value of overlapping.

To calculate the percentage of overlap, the elementary cell is used as reference, considering the red part as the yarn overlapping (Figure 2.2).
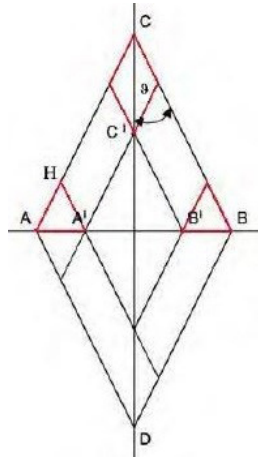
Figure 2.2: Overlapping of yarn [11]

Using the symmetry, the percentage of overlap can be defined as:

$$\%S = 100 \frac{4A_{AHA'}}{A_{ABC}} \tag{2.8}$$

Now, geometrically, it is possible to calculate the base (b) and the height (h) of the triangle AHA':

$$b = AA' = \frac{W_y}{2\cos\theta} \tag{2.9}$$

$$h = \frac{1}{2}CC' = \frac{1}{2}\frac{AA'}{\tan\theta} = \frac{1}{2}\frac{W_y}{2\cos\theta\tan\theta} = \frac{W_y}{4\sin\theta} \tag{2.10}$$

36

The overlapped area will result:

$$4A_{AHA'} = 4\frac{1}{2}bh = 4\frac{1}{2}AA'\frac{CC'}{2} = \frac{W_y^2}{4\cos\theta\sin\theta} \tag{2.11}$$

Consequently, the overlap percentage of the fibers will be

$$\%S = 100\frac{W_y^2}{4\cos\theta\sin\theta}\frac{N_c^2\tan\theta}{4\pi^2R^2} = 100\frac{W_y^2N_c^2}{16\pi^2R^2(\cos\theta)^2} \tag{2.12}$$

The maximum value of overlap percentage depends on the kind of braiding machine. Usually, it is common to avoid value over 200% so to elude the presence of too much material in axial or circumferential position that could bring the machine to lock.

2.1.2 Difference between theoretical and real cover Factor evaluation

According with the equation 2.6, the calculated cover factor could be different compared to the experimental results. Fixing the value of W_y N_c and R the graph of cover factor as a function of the braiding angle will be the one in Figure 2.3.

The curve shows an increase of the cover factor value with the braiding angle as expected, and following the equation 2.6, after the maximum value it will have a decrease. This can be explained by looking the equation of the empty space on the mandrel:

$$A_{A'B'C'} = \frac{1}{4}\left(\frac{4\pi R}{N_c} - 2\frac{W_y}{2\cos\theta}\right)^2\frac{1}{\tan\theta} \tag{2.13}$$

Once the braiding angle θ will reach the value corresponding to CF=1, the empty space on the mandrel will be zero. Increasing the braiding angle, the term in brackets will be negative, and squaring it the value of cover factor will be smaller.
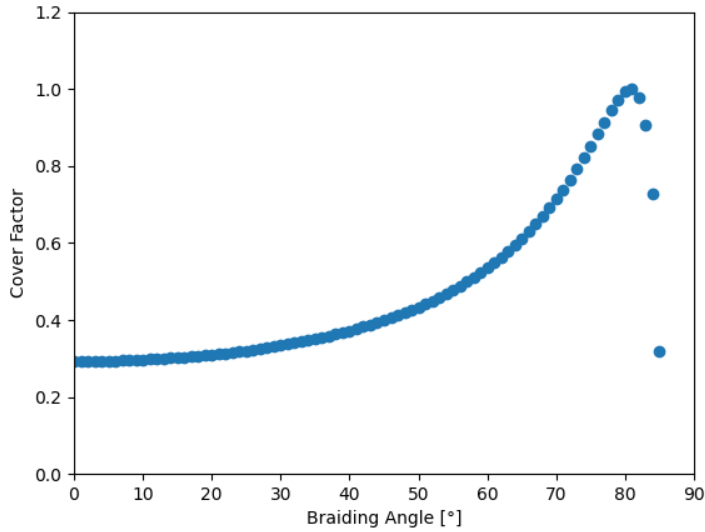
Figure 2.3: CF function of Braiding Angle obtained using equation 2.6 for biaxial braiding. It is consider a constant value for $W_y = 2mm$, $N_c = 50$, R=50mm

In reality this doesn't have any meaning since, after reaching a value equal to one, the cover factor will be constant on it. So, the Figure 2.3 will be changed (Figure 2.4 a).

The same thing can be said fixing the yarn width (W_y), the mandrel radius (R), the braiding angle (θ) and changing the cover factor as function of coils number (N_c). Using the equation 2.6 to obtain the value of the cover factor there will be a maximum value of CF and after that value, a decrease will start (Figure 2.4 b). This will not be possible considering the real physics of the problem.
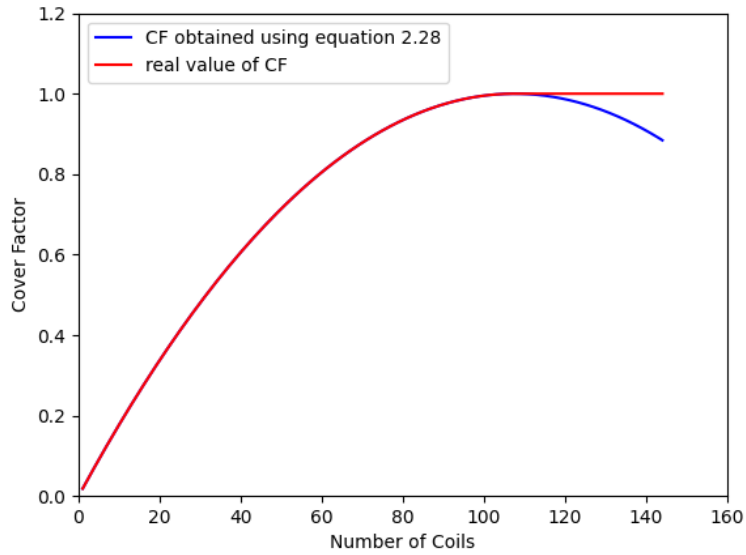
(a)
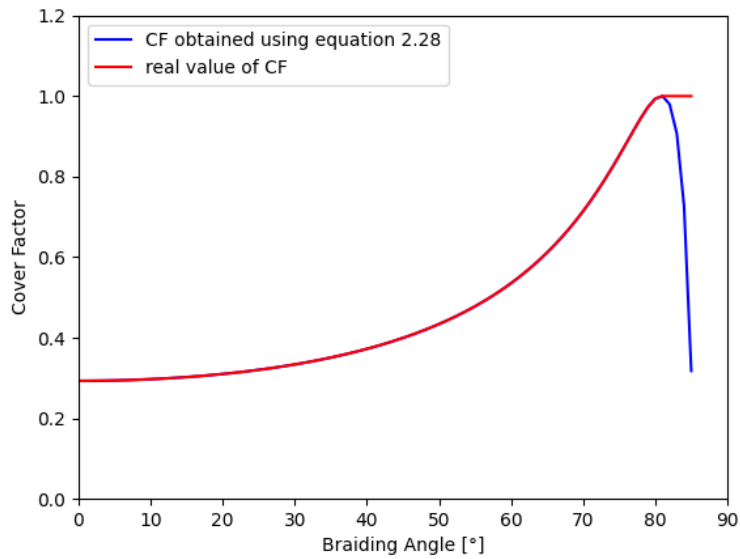
(b)

Figure 2.4: Comparison between Cover Factor of a biaxial braided preform: a) function of number of coils (Wy = 2mm, θ=70°, R=50mm); b) function of braiding angle (Wy = 2mm, Nc = 50, R=50mm)

.

The equation 2.6 gives good results, close to experimental value if the cover factor is less than one. It is possible to validate these equations producing a braided biaxial preform with hemp fibres and using the following value:

- Mandrel radius R=50mm

- Braiding Angle θ=30°

- Yarn width W_y=2mm

- Number of used coils N_c=144

Using the equation 2.6 the value of the cover factor will be CF=0.778, value not close to 1.

To evaluate the real value of CF was used the software ImageJ comparing the images turned into black and white.

The considered area is 100x100 $[mm^2]$ and is represented by the yellow square in the Figure 2.5. At this point, it is possible to obtain the number of pixels for each kind of grey and, making a subdivision between the pixels for the black colour, it will be possible to calculate the cover factor. The number of black pixels will be 612979, the number of white pixels will be 2249885, so:

$$CF_{real} = \frac{WhitePixels}{TotalPixels} = \frac{2249885}{2249885 + 612979} = 0.786 \qquad (2.14)$$

So, the difference between the real value and the calculated one will be:

$$\% = \frac{CF_{theoretical} - CF_{real}}{CF_{real}} = 1 \qquad (2.15)$$

Such small error means that the theoretical formulation of cover factor gives a good prevision of the value if it will be less than one, otherwise it is possible to consider directly CF=1.
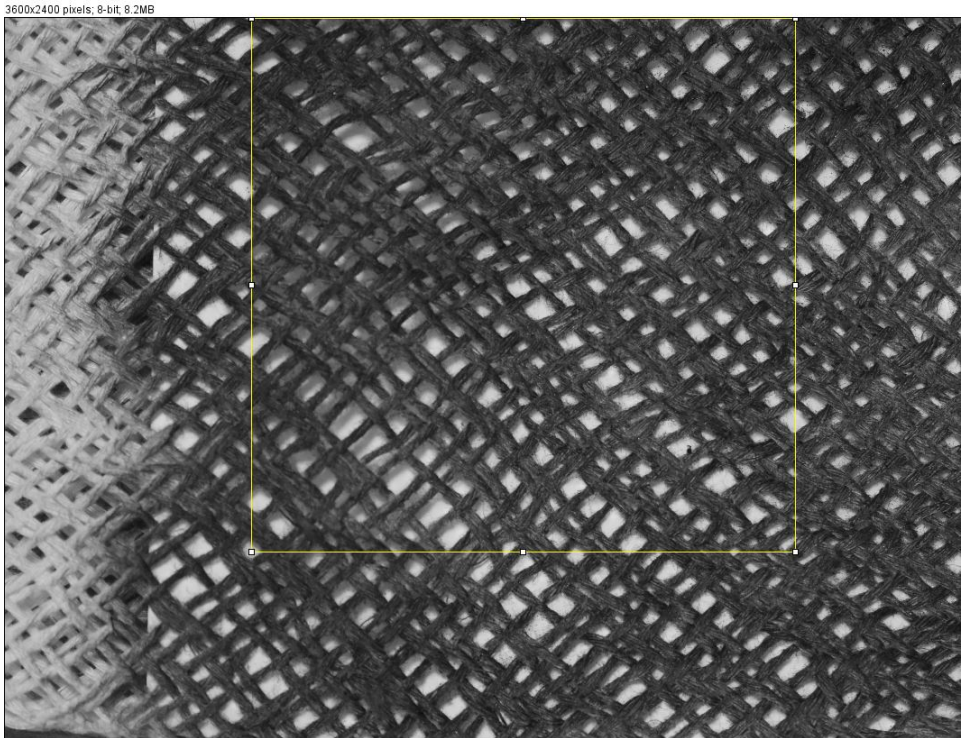
Figure 2.5: Elaboration of preform's image using ImageJ

2.2 2D Triaxial Braided preforms

Meanwhile for variables such as lay length and percentage of overlap the equations are the same for biaxial and triaxial braided preforms, for the calculation of the cover factor it is necessary to do some clarification.

In addition to the coils that are placed in the rotating part of the machine, other coils will be placed in a fixed part of the machine and they allow to add longitudinal yarns to the preform. Considering that N_c rotating coils on the machine allows to have $N_c/2$ unit cells on the mandrel, and considering that in one unit cell there will be only one axial yarn, the final number of fixed coils (N_{cL}) will be

$$N_{cL} = \frac{N_c}{2} \qquad (2.16)$$

At this point, it is possible to say that the cover factor of a triaxial braided preform will be a function of:

- Width of the yarn W_y[mm];

- Number of rotating coils N_c;

- Mandrel Radius R[mm];

- Braiding Angle θ[rad].

To calculate the cover factor it will be used a *"classical"* approach with formulation of some hypothesis, but it will be possible to notice the limitation of this approach.

2.3 Calculation of Cover Factor with a Classical Approach

This kind of analytical process is based on two fundamental hypothesis:

1. All the yarns are geometrically equal, in particular W_y is the same for everyone.

2. Longitudinal yarns are in the centre of the unit cell

In Figure 2.6 it is possible to see the new configuration of the unit cell
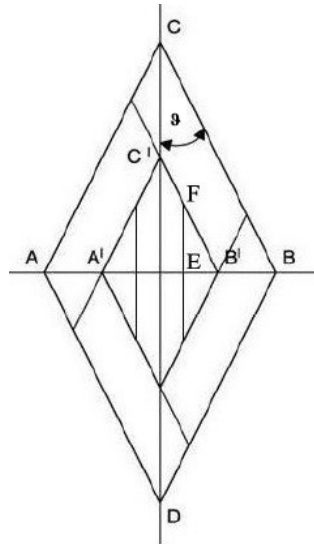
Figure 2.6: Triaxial Braided unit cell in agreement with hypothesis

As in the previous case, also here it is considered that the value of the cover factor for a single unit cell is the same as the total Braided preform. Using the symmetry of the cell, it is possible consider only the superior half of the unit cell and calculate the area of that triangle.

$$A_{ABC} = \frac{1}{2}\left(\frac{4\pi R}{N_c}\right)\left(\frac{4\pi R}{2N_c \tan\theta}\right) = \frac{4\pi^2 R^2}{N_c^2 \tan\theta} \qquad (2.17)$$

The space without yarn in the unit cell is $2A_{EB'F}$

So the base of the triangle EB'F will be:

$$
\begin{aligned}
EB' &= \frac{AB}{2} - BB' - \frac{W_y}{2} = \frac{1}{2}\frac{4\pi R}{N_c} - \frac{W_y}{2\cos\theta} - \frac{W_y}{2} = \\
&= \frac{1}{2}\left(\frac{4\pi R}{N_c} - \frac{W_y}{\cos\theta} - W_y\right)
\end{aligned}
\tag{2.18}
$$

where the value of AB was calculated in equation 2.1.

Now it is possible to obtain the height EF of the same triangle

$$
EF = EB'\cot\theta = \frac{EB'}{\tan\theta} = \frac{1}{2}\left(\frac{4\pi R}{N_c} - \frac{W_y}{\cos\theta} - W_y\right)\frac{1}{\tan\theta}
\tag{2.19}
$$

It is clear that the area of the half of the unit cell without yarns will be

$$
\begin{aligned}
2A_{EB'F} &= 2\frac{1}{2}(EB'\cdot EF) = \frac{EB'^2}{\tan\theta} = \frac{1}{4}\left(\frac{4\pi R}{N_c} - \frac{W_y}{\cos\theta} - W_y\right)^2\frac{1}{\tan\theta} = \\
&= \frac{1}{4\tan\theta}\left(\frac{16\pi^2 R^2(\cos\theta)^2 + W_y^2 N_c^2(1+(\cos\theta)^2)}{N_c^2(\cos\theta)^2} - \right. \\
&\qquad\left. - \frac{8W_y N_c\pi R\cos\theta(1+\cos\theta) + 2W_y^2 N_c^2\cos\theta}{N_c^2(\cos\theta)^2}\right)
\end{aligned}
\tag{2.20}
$$

The cover factor will be the complementary of not covered area

$$
\begin{aligned}
CF = 1 - \frac{2A_{EB'F}}{A_{ABC}} = \\
= 1 - \left(1 - \frac{W_y N_c [8\pi R \cos\theta (1 + \cos\theta)}{16\pi^2 R^2 (\cos\theta)^2} - \right. \\
\left. - \frac{W_y N_c (1 + (\cos\theta)^2 + 2\cos\theta)]}{16\pi^2 R^2 (\cos\theta)^2} \right)
\end{aligned}
\tag{2.21}
$$

As done for the biaxial braided preform, also in this case it is possible to calculate the cover factor using fixed parameters. Same parameters of the biaxial example will be used:

- Mandrel radius R=50mm

- Braiding Angle θ=30°

- Yarn width W_y=2mm

- Number of rotating coils N_c=144,

- Number of fixed coils N_{cL}=72

Using the equation 2.21 the cover factor will result 0.999, obviously more than the value of the biaxial preform (CF=0.778) due to the presence of longitudinal yarns. As the biaxial preform, also the formulation for the triaxial case presents a cover factor that, in function of the braiding angle or number of coils, reaches the maximum value equal to 1 and after that it starts to decrease; also in this case, the real value of the cover factor after the maximum value is different from the analytical one (Figure 2.7).
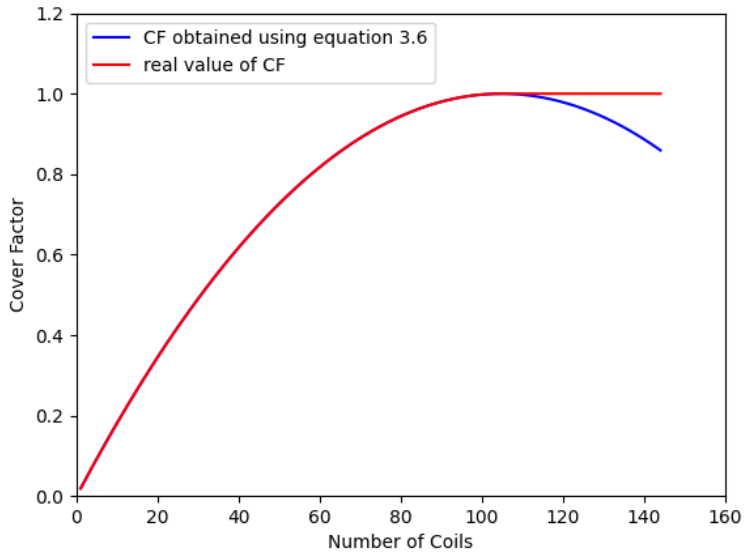
(a)
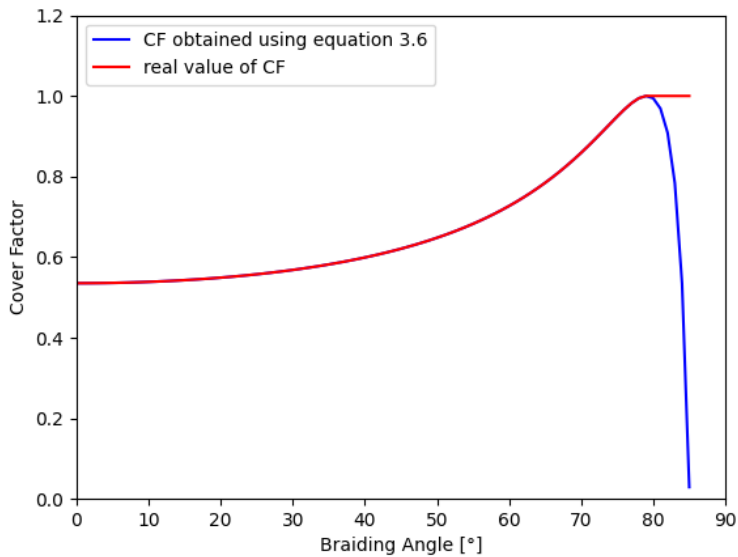
(b)

Figure 2.7: Comparison between Cover Factor of a triaxial braided preform, obtained using equation 2.21 and the real one: a) function of number of coils ($W_y = 2mm$, θ=70°, R=50mm); b) function of braiding angle ($W_y = 2mm$, $N_c = 50$, R=50mm)

46

It is possible to obtain the limit condition of CF=1 considering the empty area equal to 0, so EB'=0 and A'B'=W_y, but A'B' will be also:

$$A'B' = AB - AA' - BB' = \frac{4\pi R}{N_c} - \frac{W_y}{2\cos\theta} - \frac{W_y}{2\cos\theta} = \frac{4\pi R}{N_c} - \frac{W_y}{\cos\theta}$$
(2.22)

Knowing the braiding angle θ and the yarn width, it is possible to know the value R_{min}, which is the minimum value of the radius to obtain a value of CF equal to 1. For a radius of the mandrel smaller than the value R_{min} there will be an overlap of yarns.

$$W_y = \frac{4\pi R}{N_c} - \frac{W_y}{\cos\theta}$$

$$W_y = \frac{4\pi R\cos\theta - W_y N_c}{N_c \cos\theta}$$
(2.23)

$$W_y N_c (1 + \cos\theta) = 4\pi R\cos\theta$$

$$R_{min} = \frac{W_y N_c (1 + \cos\theta)}{4\pi\cos\theta}$$

In 2017 a software that permits to design braided preforms using a circular mandrel was developed, considering all the equation that have been described previously[17]. Melenka and Carey described in detail the mathematical model used in different software for the calculation of the braiding parameters [41] [42]. Using these kinds of software it is possible to compare the mechanical properties with the braiding geometry. In fact, due to the high number of parameters and the different combinations, a trial and error approach would be really expensive.

The problem is that only for simple geometry it is possible to use an analytical approach, while for something more complex the mathematical model evolves in a problematic way [43]. To solve this problem, in recent years many Finite Element software were developed with the aim to simulate the process with an high accuracy, although they have an elevated computational time even using a work station [13]. In order to save time in the design, it is better to use software based on the solution of cinematic equations, but it is necessary not to limit the study only to the axisymmetric preform. Michaeli et al.[44] studied non circular mandrels using the rotation velocity of the horn gears ω as an input parameter and the feed speed of the mandrel as an output. Gao et al.[45] theorized a software with the possibility of modelling axisymmetric preform using as inputs the typology of braid, the number of coils and the parameters of the yarn (density, engineering constant, and width-thickness ratio). In the last years, two software for the braiding simulation were developed: "TexMind Braider Standard" and "TexMind Braiding Configurator" [46]. The last software is a cinematic one and was developed by van Ravenhorst in the university of Twente; its name is "Braidsim" and it simulates the movement of biaxial and triaxial braiding providing as output also a Finite Element Model for the interface with other software and the mechanical analysis [47].

2.3.1 Tool for designing braided preform

Using a programming software, it was developed an indoor tool with all the equations presented in this chapter to calculate the unit cells and to predict the process parameters of preforms obtained with a Circular Braiding Machine.

In the Figure 2.8 it is possible to notice the graphical user interface of the tool, where there are also all the variables and the geometrical data of the fibres.
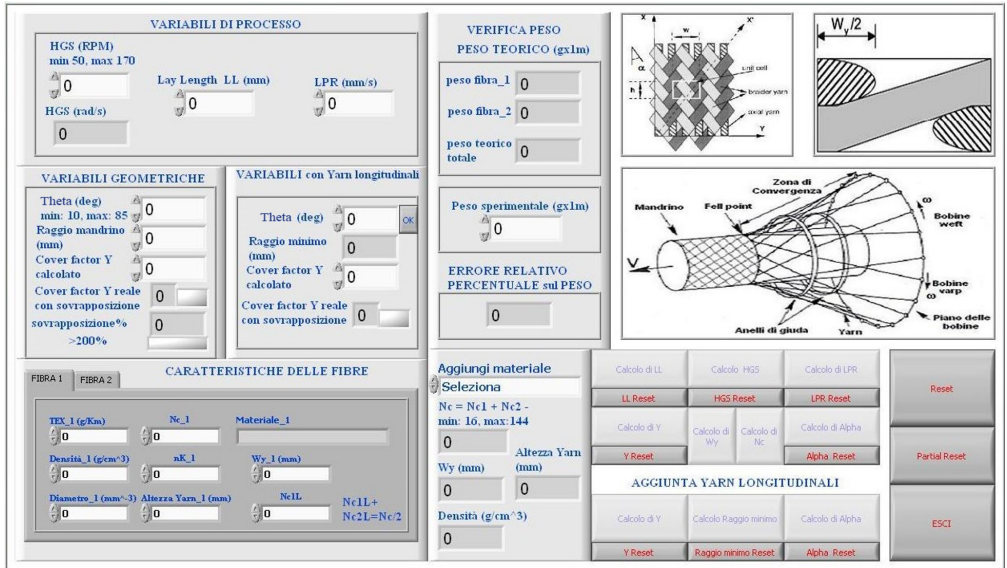
Figure 2.8: Developed Tool

In the following Figure (Figure 2.9) there is an example where is implemented the calculation of the cover factor in the "Block Diagram" of the software.
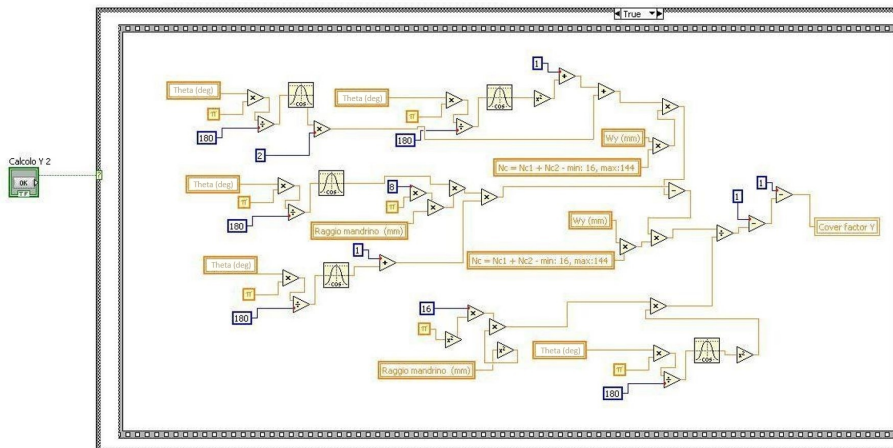
Figure 2.9: Partial back-panel of Developed Tool

In Figure 2.10 there is a block diagram that describes how the tool works:
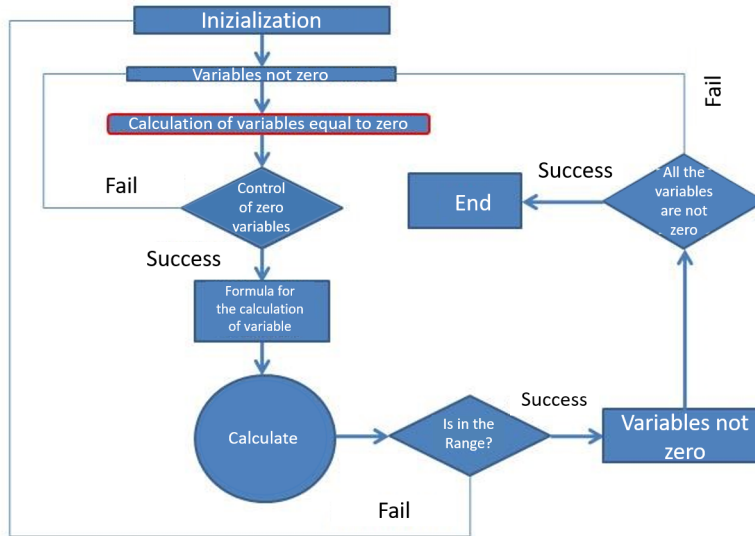
Figure 2.10: Block Diagram to explain how the tool works

1. Insert the known variables in the tool

2. The software will recognize which kind of equation to use to calculate the unknown variables and will light a button for the calculation

3. Starting from a variable that is calculated, it will be possible to obtain the others in consequence

4. When there will be a variable out of range there will be an error message

It is important to observe the technological ranges of validity of the parameters in the case of the used machine (Herzog RF 1/144-100)

$$10° < \theta < 85°$$
$$50[rpm] < HGS < 170[rpm]$$
$$16 < N_c \leq 144$$

In the event that the braiding angle is less than 10° it would not be possible to cover the surface of the spindle and you would have a blockage by longitudinal overlap of the fibers. If the value of the braiding angle is greater than 85° there will be an overlap of the fibers in the transverse direction to the spindle and, again, it will cause the braiding to lock. HGS speed limits are physical limits of the machine.

This tool permit also to use different kinds of fibres to obtain hybrid preforms and balance the mechanical properties of the final product. The developed model for the calculation of geometrical parameters in the tool uses two cards to describe the two different used materials. In this case, the width of the yarn will be calculated using an average of the value of the single yarns:

$$W_y = \frac{N_{c1}}{N_c} \cdot W_{y1} + \frac{N_{c2}}{N_c} \cdot W_{y2}$$

There is a library where common materials are listed and it is possible to use one of these in the equation with all its geometrical properties (Figure 2.11).

In Figure 2.12 it is possible to notice what happens to the tool using a value of mandrel radius equal to 80mm and a braiding angle of 45°. As said before it is possible to see that the values are correct to realize the preform and so the light will become green.
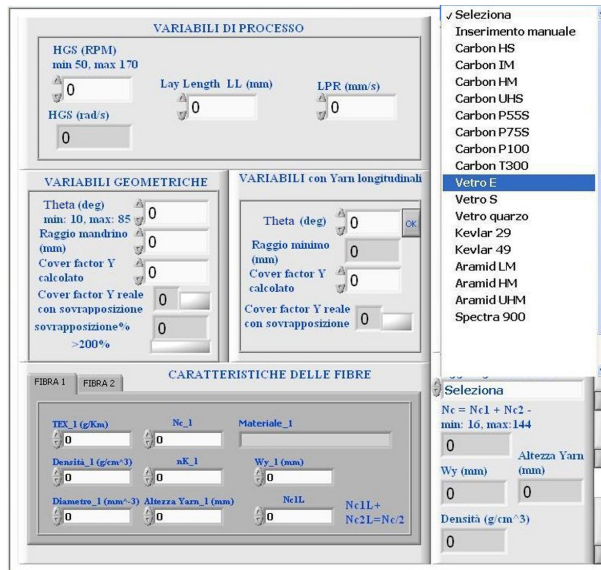
Figure 2.11: Library with materials geometrical properties

Figure 2.12: Screen of the tool using R=80mm and θ=45° with the presence of longitudinal yarn

All these models (mathematical or cinematic modelling) and the developed tool keep in consideration the value of cover factor calculated with the previous equations, but during the production of triaxial braided preform, ImageJ software was used to make a comparison between the analytical value of cover factor and the real one (as for the biaxial preform case). From the results, it was clear that the difference between the two values was high, and making an accurate visual inspection, results clear that the two hypothesis are not respected. Indeed, it is possible that the longitudinal yarns are not passing for the centre of the unit cell how confirmed by experimental process. It is necessary to find another mathematical model to describe the value of the cover factor for a triaxial braided preform.

2.4 Different configurations of longitudinal yarns in the unit cell

As said previously, the hypothesis that the longitudinal yarns pass in the centre of unit cell is a big approximation that brings to an error when the cover factor is analytically calculated. Heieck et al. [29] described a way to find a cover factor that is better matched with an experimental value.

Below it is possible to check the variable used for this calculation:

- Braiding angle θ

- Width of warp and weft yarns W_y

- Width of longitudinal yarn W_{yL}

- Number of rotating coils N_c

- Mandrel radius R.

There is another parameter that can be seen in Figure 2.13
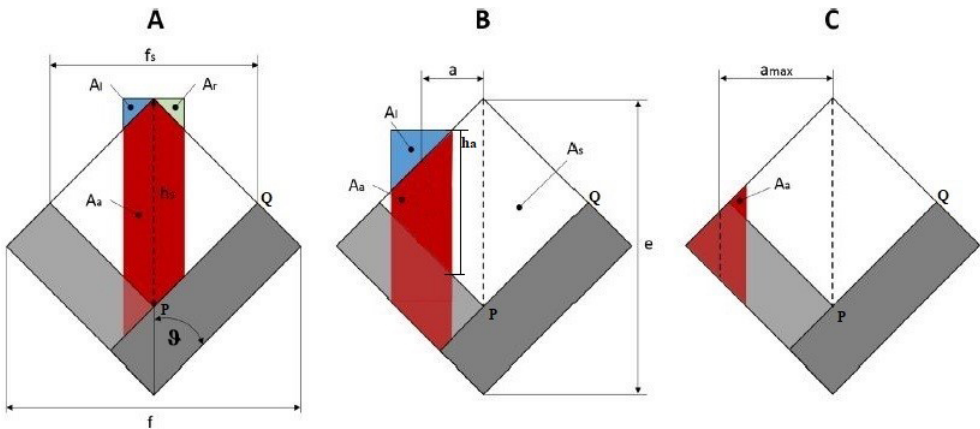
Figure 2.13: Different configuration of longitudinal yarn in unit cell [29]

"a" represents the distance between the centre of the unit cell and the axis of the longitudinal yarn. Changing a there will be three different cases. Also in this situation, the unit cell will be a rhombus, so its total area will be

$$A = \frac{1}{2} e \cdot f \tag{2.24}$$

with f equal to the value of AB for the biaxial unit cell

$$f = \tfrac{4\pi R}{N_c}$$

and e equal to

$$e = f \cot \theta$$

Now, it will be easy to calculate PQ from geometrical value:

$$PQ = \frac{f}{2\sin\theta} - \frac{W_y}{\sin 2\theta} = \frac{\pi D}{N_c \sin\theta} - \frac{W_y}{\sin 2\theta} \tag{2.25}$$

Knowing PQ it is possible to calculate the internal diagonal of the rhombus (f_s, h_s)

$$f_s = 2PQ\sin\theta = 2\left(\tfrac{\pi D}{N_c \sin\theta} - \tfrac{W_y}{\sin 2\theta}\right)\sin\theta$$

$$h_s = 2PQ\cos\theta = 2\left(\tfrac{\pi D}{N_c \sin\theta} - \tfrac{W_y}{\sin 2\theta}\right)\cos\theta$$

At this point the area of the internal cell is

$$A_s = \frac{1}{2} h_s \cdot f_s = \frac{1}{2} 4 \left(\frac{\pi D}{N_c \sin\theta} - \frac{W_y}{\sin 2\theta}\right)^2 \sin\theta\cos\theta =$$
$$= \left(\frac{\pi D}{N_c \sin\theta} - \frac{W_y}{\sin 2\theta}\right)^2 \sin 2\theta \tag{2.26}$$

Now it is necessary to obtain the area occupied by the longitudinal yarn A_a. For this purpose, there are three different cases (Figure 2.13).

Case A

In this case, the longitudinal yarn passes from both the symmetric side of unit cell (Figure 2.14)
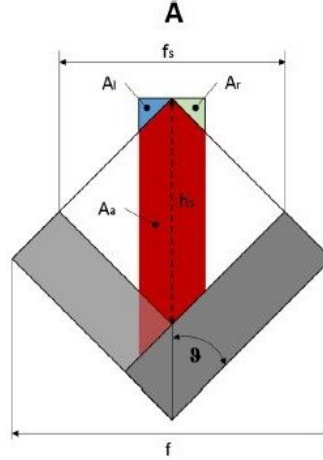
Figure 2.14: Unit cell typology A

The value of a will be

$$0 \leq a \leq \frac{W_{yL}}{2}$$

Now it will be necessary to calculate the rectangular area of the yarn with base W_{yL} and height h_s

$$
\begin{aligned}
W_{yL} \cdot h_s &= W_{yL} 2 \left(\frac{\pi D}{n \sin \theta} - \frac{W_y}{\sin 2\theta} \right) \cos \theta = \\
&= W_{yL} 2 \left(\frac{\pi D \cos \theta}{N_c \sin \theta} - \frac{W_y}{2 \sin \theta \cos \theta} \cos \theta \right) = \\
&= W_{yL} \left(\frac{2\pi D}{N_c} \cot \theta - \frac{W_y}{\sin \theta} \right)
\end{aligned}
$$

From this value, subtracting the value of the blue area A_l(two times) and the green area A_r (two times), we get the value of the area occupied by the longitudinal yarn

56

$$2A_l = 2\left[\frac{1}{2}\left(\frac{W_{yL}}{2}+a\right)\left(\frac{W_{yL}}{2}+a\right)\cot\theta\right] = 2\frac{\left(\frac{1}{2}W_{yL}+a\right)^2}{2}\cot\theta$$

$$2A_r = 2\left[\frac{1}{2}\left(\frac{W_{yL}}{2}-a\right)\left(\frac{W_{yL}}{2}-a\right)\cot\theta\right] = 2\frac{\left(\frac{1}{2}W_{yL}-a\right)^2}{2}\cot\theta$$

$$A_a = \cot\theta\left(\frac{2\pi D}{N_c}W_{yL} - \frac{1}{2}W_{yL}^2 - 2a^2\right) - \frac{W_y W_{yL}}{\sin\theta} \qquad (2.27)$$

Case B

This is the condition in which the yarn is only on one side of the unit cell without passing through the value of f_s (Figure 2.15). The condition for "a" is:

$$\frac{W_{yL}}{2} \leq a \leq \frac{f_s}{2} - \frac{W_{yL}}{2}$$
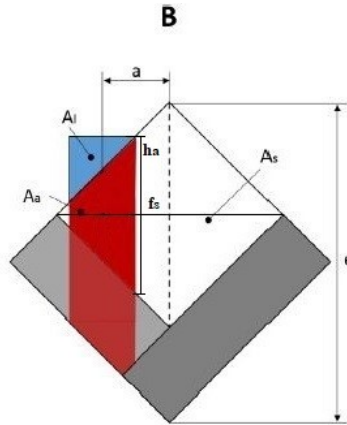
Figure 2.15: Unit cell typology B

Obviously, this case exists only if $W_{yL} \leq \frac{f_s}{2}$ is respected. This means that the number of rotating coils N_c has to be not high, consequently, the number of the unit cell will be small enough to allow the existence of case B. Otherwise, the typology A will be extended in a wide range.

It is possible to calculate the limit value of N_c:

$$\frac{f_s}{2} = W_{yL}$$

$$\left(\frac{\pi D}{N_c \sin \theta} - \frac{W_y}{\sin 2\theta} \right) \sin \theta = W_{yL}$$

$$N_{c1} = \frac{2\pi D \cos \theta}{2W_{yL} \cos \theta + W_y} \tag{2.28}$$

Hypothesizing the validity of the condition $N_c \leq N_{cL}$ it is possible to calculate the value of A_a for this case.

The rectangular with the dimension W_{yL} and h_a will have an area equal to:

$$h_a W_{cL} = [h_s + (W_{cL} - 2a) \cot \theta] W_{cL}$$

From this area it is necessary to subtract the blue triangle area A_l

$$2A_l = 2 \left[\tfrac{1}{2} W_{yL} W_{yL} \cot \theta \right] = W_{yL}^2 \cot \theta$$

$$A_a = [h_s + (W_{cL} - 2a) \cot \theta] W_{cL} - W_{yL}^2 \cot \theta = W_{yL}(h_s - 2a \cot \theta) \tag{2.29}$$

Case C

In this case, the longitudinal yarn overlaps the braided yarn on the symmetric axis f_s (Figure 2.16)

The condition for the existence of this case is:

$$\frac{f_s}{2} - \frac{W_{yL}}{2} \leq a \leq a_{max}$$

where $a_{max} = \frac{f}{2} - \frac{W_{yL}}{2}$
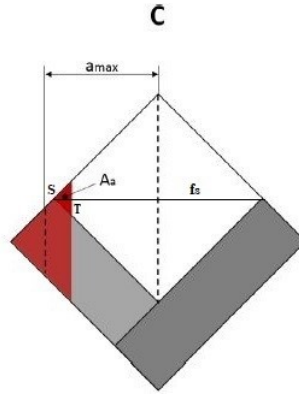
Figure 2.16: Unit cell typology C

The area occupied by the longitudinal yarn will be equal to the triangle with heigh ST.

$$ST = \frac{f_s}{2} - a + \frac{W_{yL}}{2}$$

Consequently, the base of the triangle is $2 \cdot ST \cot \theta$. From this it will be possible to calculate the area

$$A_a = \frac{1}{2}\left(\frac{f_s}{2} - a + \frac{W_{yL}}{2}\right) 2\left(\frac{f_s}{2} - a + \frac{W_{yL}}{2}\right) \cot \theta = \left(\frac{f_s}{2} - a + \frac{W_{yL}}{2}\right)^2 \cot \theta$$

$$(2.30)$$

Cover Factor

Following the literature [29] it is possible to evaluate the cover factor using the equations in Tables 2.1 and 2.2 to calculate the occupied area by the longitudinal yarn in different configurations.

Table 2.1: Summarizing of calculation of longitudinal yarn area including the existence of Case B ($\frac{f_s}{2} > W_{yL}$)

	Value of a	A_a
A	$0 \leq a < \frac{W_{yL}}{2}$	$\cot\theta\left(\frac{2\pi D}{N_c}W_{yL} - \frac{1}{2}W_{yL}^2 - 2a^2\right) - \frac{W_y W_{yL}}{\sin\theta}$
B	$\frac{W_{yL}}{2} \leq a < \frac{f_s}{2} - \frac{W_{yL}}{2}$	$W_{yL}(h_s - 2a\cot\theta)$
C	$\frac{f_s}{2} - \frac{W_{yL}}{2} \leq a \leq \frac{f}{2} - \frac{W_{yL}}{2}$	$\left(\frac{f_s}{2} - a + \frac{W_{yL}}{2}\right)^2\cot\theta$

Table 2.2: Summarizing of calculation of longitudinal yarn area without Case B ($\frac{f_s}{2} < W_{yL}$)

	Value of a	A_a
A	$0 \leq a < \frac{f_s}{2} - \frac{W_{yL}}{2}$	$\cot\theta\left(\frac{2\pi D}{N_c}W_{yL} - \frac{1}{2}W_{yL}^2 - 2a^2\right) - \frac{W_y W_{yL}}{\sin\theta}$
C	$\frac{f_s}{2} - \frac{W_{yL}}{2} \leq a \leq \frac{f}{2} - \frac{W_{yL}}{2}$	$\left(\frac{f_s}{2} - a + \frac{W_{yL}}{2}\right)^2\cot\theta$

The final cover factor will be defined as:

$$CF = \frac{A + A_a - As}{A} \tag{2.31}$$

Knowing the cover factor of triaxial unit cell, it is possible to calculate the cover factor of the entire preform. Considering the hypothesis that all the longitudinal yarns are placed in an equal way in all the unit cells (a has the same value for all the cells), the CF of the entire preform will be the same as the cover factor of the unit cell.

Making a comparison between the value calculated with the equation 2.31 and the experimental value of cover factor, it is clear that there is a not negligible error. In the following Chapter it will be discussed about the error and a possible solution.

Chapter 3

New approach for Cover Factor Calculation

During the experimental part of this work, it was produced with a Radial Braiding Machine a Triaxial braided preform with the following parameters:

- Braiding angle θ=30°

- Mandrel Radius R=50mm

- Number of rotating coils N_y=72

- Number of longitudinal coils $N_{yL} = N_y/2$=36

In Figure 3.1 it is possible to see the final product:

Figure 3.1: Triaxial braided product with R=50mm, θ=30°, N_y=72, N_{yL}=36

From optical measurements it will result that the rotating yarns will have a width in the range 1.8mm and 2.2mm, meanwhile the longitudinal yarns will have a width between 1.8mm and 2mm. It was decided to fix a value of W_y=2mm and W_{yL}=2mm.

As done for the biaxial preform, also in this case the real value of cover factor was found with a software used for the elaboration of the images called ImageJ. Painting the preform in black and using a white background the image in the software was converted in greyscale (Figure 3.2)
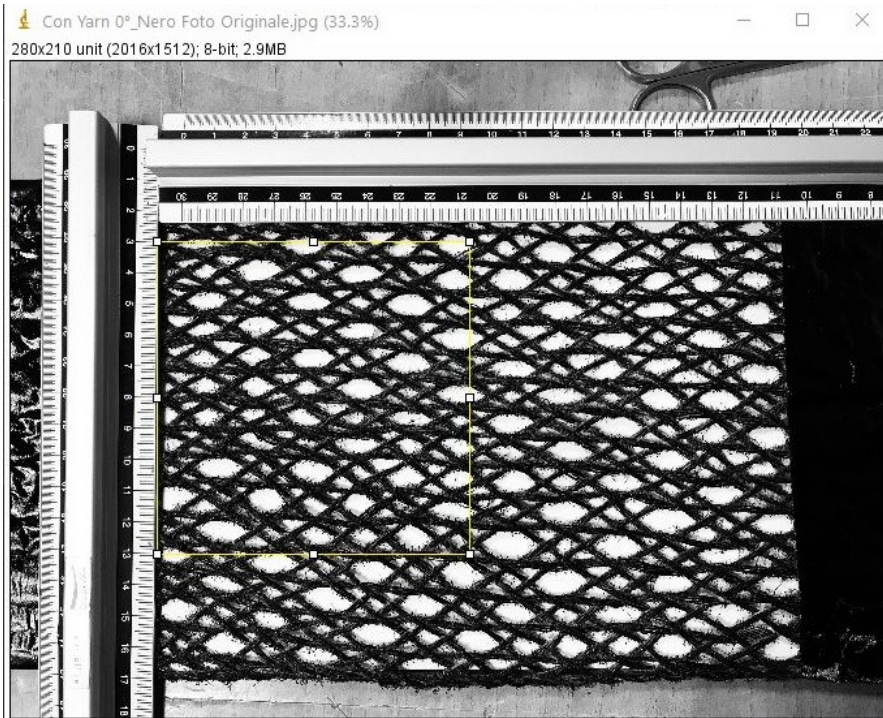
Figure 3.2: Triaxial braided preform with R=50mm, θ=30°, N_y=72, N_{yL}=36 analyzed in the ImageJ software

The analysed area is equal to 10000 mm^2 for a total number of 518400 pixels. The black pixels, representing the yarn, resulted to be 323116, consequently the real value of cover factor was:

$$CF_{real} = \frac{BlackPixels}{TotalPixels} = \frac{323116}{518400} = 0.623$$

Analysing the production parameters (θ, R, W_y, W_{yL}), it is possible to obtain the maximum value of N_c to understand in which of the case studie we are (A,B,C or A,C).

$$N_c = 99.6$$

This value is higher than the number of rotating coils used for the production of braided preforms ($N_c = 76$). From Figure 3.1 it is possible to notice that the longitudinal yarns are not placed in the same way for each cell, so the value of a parameters will not be the same, and there will be 3 kinds of unit cells (typology A, typology B, typology C). The problem is the impossibility to know from the beginning the number of each typology of unit cell, and at the same way triaxial preforms realized with same process parameters can give as results different percentage of unit cells typologies.
To solve this problem, it is used as a way to simulate a high number of produced preforms with the same process parameters, but with different percentages of cells typologies generated in a random way.

In Table 3.1 it is possible to see the first 10 random simulations. The total number of simulations is 5000, since it was checked that this number is enough to reach a stability of cover factor value (Figure 3.3)

Table 3.1: Example of first 10 simulation of produced preform with random distribution of cells typology

A	B	C	Sum
66	16	18	100
71	5	24	100
50	40	10	100
3	91	6	100
12	53	35	100
15	51	34	100
53	44	3	100
45	3	52	100
57	12	31	100
66	7	27	100
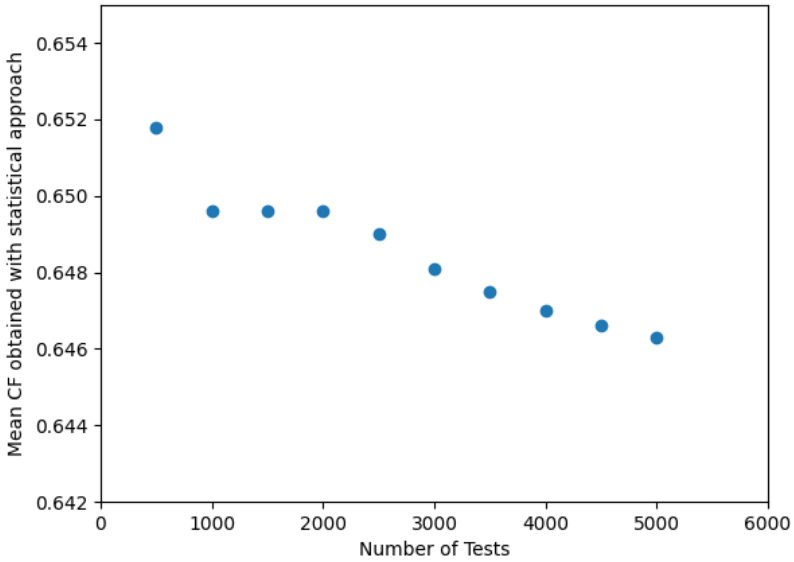
Figure 3.3: Evolution of value of cover factor in function with the number of simulations for the preform realize with following parameters: R=50mm, $\theta=30°$, $N_y=72$, $N_{yL}=36$

In Table 3.2 are reported the geometrical parameters of the cells that are not depending on the typology of the cells, but only from the production parameters and from the typology of fibres.

Table 3.2: Geometrical parameters obtained with a process using R=30mm, θ=30°, N_y=72, N_{yL}=36 and hemp fibres

f	8.72664626
e	15.1149947
A	65.95160599
f_s	6.417245183
h_s	11.1149947
A_s	35.66382311

In Table 3.3 and 3.4 it is possible to see the different ranges of parameter a for different typologies of cell and the value of cover factor calculated for each case:

Table 3.3: Value of a for different typologies of cells, obtained with a process using R=30mm, θ=30°, N_y=72, N_{yL}=36 and hemp fibres

a		
Min	**Max**	**Typology**
0	1	A
1	2.208622592	B
2.2086226	3.36332313	C

Table 3.4: Value of CF for different typologies of cells, obtained with a process using R=30mm, θ=30°, N_y=72, N_{yL}=36 and hemp fibres

Condition	Value of a	Typology	A_a	CF
$a=0$	0	A	18.766	0.744
$a=\frac{f_s}{4}$	1.604	B	11.115	0.628
$a=a_{max}$	3.363	C	1.238	0.478

From Table 3.4 it is clear that:

- The condition for typology A considers the longitudinal yarn perfectly centred

- The condition for typology B considers the longitudinal yarn in the centre of one part of the cell

- The condition for typology C considers the longitudinal yarn in the extreme location of the cell

In the end the value of Cover Factor will be a weighted average of different factors of different typologies

$$CF_{preform} = \frac{\%_A \cdot CF_A + \%_B \cdot CF_B + \%_C \cdot CF_C}{100}$$

For example the first row of Table 3.1 (%A=0.66,%B=0.16,%A=0.18) will give a value of CF=0.67. Making this procedure for all the 5000 simulation it will be possible to consider the value of cover factor equal to the average value of the simulations. In this case the final value will be CF=0.646

As seen, the classical approach using the equation 2.21 to calculate the cover factor will give a value of CF=0.744 with a percentage deviation of 19.4% respect the real value of CF=0.623; instead using this new approach and considering all the listed variables the percentage deviation will be only of 3.7%.

3.0.1 Other considerations about the number of coils

At this point it will be necessary to evaluate the influence of the number of coils, used for the production, on the value of the cover factor calculated with this new approach. As expected, increasing the number of coils there will be more materials and therefore the cover factor will increase.

In Table 3.5 it is possible to see all the possible configurations to set the used machine; the last row represents the full equipped machine.

Table 3.5: Possible configuration of the RF 1/144-100 machine

Rotating Coils	Warp Coils	Weft Coils	Fixed Coils
4	2	2	2
6	3	3	3
12	6	6	6
16	8	8	8
18	9	9	9
24	12	12	12
36	18	18	18
48	24	24	24
72	36	36	36
96	48	48	48
108	54	54	54
120	60	60	60
126	63	63	63
128	64	64	64
132	66	66	66
136	68	68	68
138	69	69	69
140	70	70	70
144	72	72	72

As previously analysed, the influence of number of coils on the typology of cells could change the way to calculate the cover factor; especially in the case in which $N_c > N_{c1}$. In this event, the typology B will not exist, so the value of CF cannot be calculated statistically considering the average on three typologies of cells, but only using cell A and cell C.

$$CF_{preform} = \frac{\%_A \cdot CF_A + \%_C \cdot CF_C}{100} \qquad (3.1)$$

In the case in which the number of coils and the braiding angle are really high, the yarns will result close and they will cover all the mandrel, so the cover factor will be one. Also in this case, we can obtain the maximum value of N_c beyond which the cover factor will be 1.

$$\frac{f_s}{2} = \frac{W_{yL}}{2}$$

This means that if the yarn is in the center of the unit cell (a=0) it will cover the whole mandrel occupying the empty space of the cell. Substituting $\frac{f_s}{2}$

$$\left(\frac{\pi D}{N_c \sin \theta} - \frac{W_y}{\sin 2\theta} \right) \sin \theta = \frac{W_{yL}}{2}$$

isolating N_c we will obtain the value of N_{c2} that is the limit value

$$N_{c2} = \frac{2\pi D \cos \theta}{W_{yL} \cos \theta + W_y} \qquad (3.2)$$

For the analysed case (R=50mm , $\theta = 30$, $W_y = 2mm$, $W_{yL} = 2mm$) the value of N_2 is 145.8. The maximum configuration of the machine is 144 coils, less of the maximum number of coils to obtain CF=1 with a braiding angle of 30°, so the mandrel will not be totally covered. In the following table it will be possible to notice the two limits N_1 and N_2 for the braiding angle equal to 30°, 45° and 60° using a fixed mandrel radius (R=50mm) and the fixed value of W_{yl} and W_{yL} (2mm)

Table 3.6: Limitation of N_c for different braiding angle with R, W_y and W_{yL} fixed (50mm,2mm,2mm)

θ	N_{c1}	N_{c2}
30	99.58	145.8
45	92.01	130.13
60	78.5	104.72

Summarizing

- With $N_c < N_{c1}$ the value of cover factor is calculated considering the average of the three typologies of unit cells (A, B and C)

- With $N_{c1} < N_c < N_{c2}$ the value of cover factor is calculated considering the average of only two typologies of unit cells (A and C)

- With $N_c > N_{c2}$ the value of cover factor is unitary

Considering the two Tables 3.5 and 3.6, it is possible to know how to calculate the cover factor depending on the configuration of the machine (Table 3.7)

Table 3.7: How to calculate the cover factor depending on the machine configuration

θ	Number of Coils		
30	4 to 96	108 to 144	/
45	4 to 72	96 to 128	132 to 144
60	4 to 72	96	108 to 144
	$N_c < N_{c1}$	$N_{c1} < N_c < N_{c2}$	$N_c > N_{c1}$
	CF=A+B+C	CF=A+C	CF=1

If the value of CF equal to 1 will be reached without reaching the complete number of coils on the machine, it is suggested to stop the number of coils to that value to not have overlapping fibres.

At this point it will be easy, keeping a constant value of mandrel radius, to build a graph that gives the value of cover factor as a function of the configuration of the machine (in terms of coils) for each value of braiding angle (Figure 3.4, 3.5, 3.6).
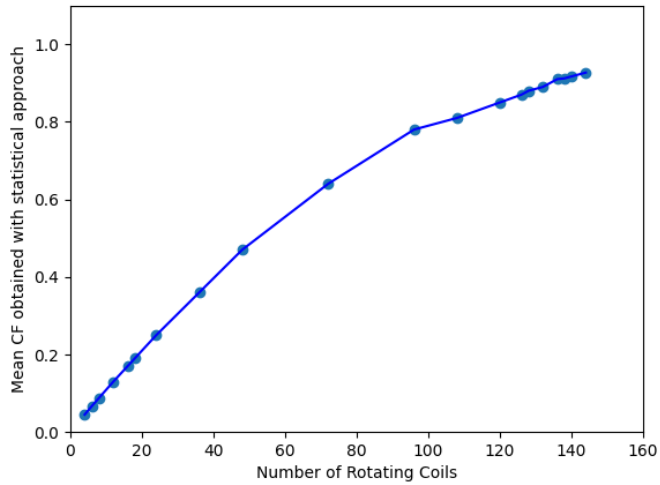
Figure 3.4: Evolution of value of cover factor in function with the number of coils used for the production with following parameters: R=50mm, θ=30°
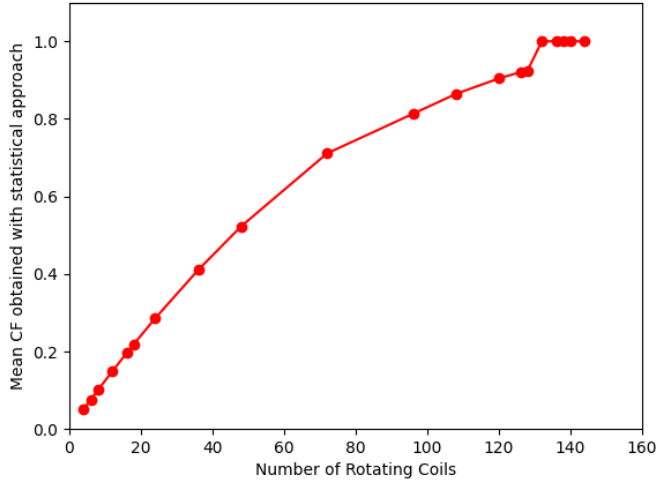
Figure 3.5: Evolution of value of Cover Factor in function with the number of coils used for the production with following parameters: R=50mm, θ=40°
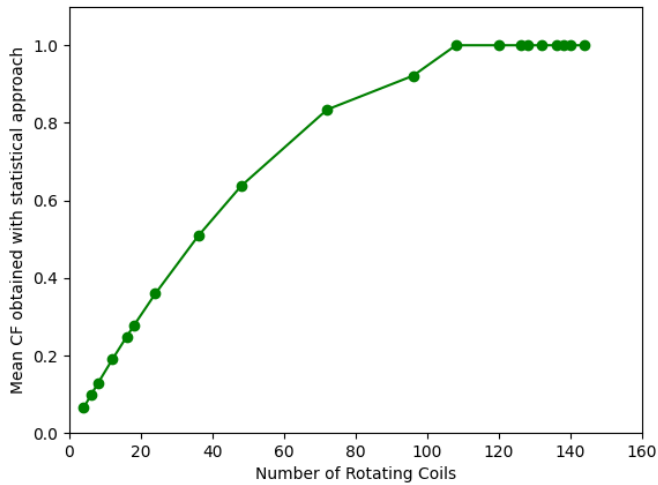
Figure 3.6: Evolution of value of cover factor in function with the number of coils used for the production with following parameters: R=50mm, θ=60°

Section III

Chapter 4

Production of Braided Preforms and Mechanical Tests

In this chapter it will be shown the production process of Braided hemp preform, the realization of the composite panels and the mechanical tests used to compare the different typologies of preforms and braiding angle used.

The main phases of the work can be summarised in:

1. Using of Radial Braiding Machine to obtain interlaced preforms

2. Infusion process with RIFT technique (Resin Infusion under Flexible Tooling)

3. Cutting of specimens and mechanical tests

4.0.1 Use of Radial Braiding Machine to interlace the preform

The Machine used to obtain the preforms is an RF 1/144-100 by Herzog. The machine was loaded with 144 rotating coils and 72 coils for the longitudinal yarns (not all the coils were used during the production process). The first step was the realization of the coils using a bobbin winding machine called SP 280-PN by Herzog. The bobbin winding machine permits to wind the coils starting from bigger spools. With this machine it is possible to wind 4 coils simultaneously (2 clockwise and 2 counterclockwise). Each coil has 100 mt of yarn winded on. In 4.1 it is possible to see the two different machines.

Figure 4.1: Herzog RF 1/144-100 and Herzog SP 280-PN

In the following figure (Figure 4.2) it is possible to see the details of the bobbin winding machine.

After the realization of the coils, they are placed on the machine and the mandrel is placed in the centre. Consequently, it is decided the configuration to use for the production and the machine is set.

Figure 4.2: Winding process of the yarns on the coils

4.0.1.1 Used Production Parameters and their control

During the set-up of the machine, some of process parameters are defined. The radius of the preform is equal to the value of the radius mandrel and in this case is fixed to 50mm. Another parameter is the one linked with the number of coils used. For the biaxial one, different configurations are used, depending from the desired braiding angle; to obtain a preform with a braiding angle of 30°, 144 rotating coils are used, while the realization of composites with an angle of 45° was performed with 120 rotating coils.

The triaxial braided preform has two configurations of the machine: the first one includes a fully loaded machine (144 rotating coils and 72 fixed coils); the second configuration provides a machine loaded with half of the total of the coils (96 rotating coils and 48 fixed coils). Obviously, the first configuration will have elevated CF. For the braiding angle the realized preforms will have θ equal to 30° and 45°. Fixing R and θ, it will be possible to calculate the value of Lay Length (LL) using equation 1.15, and, putting this value in the machine, the desired preform will be obtained. In the following Table (Table 4.1) it is possible to see all the production parameters for all the realized preforms, including the calculated Cover Factor.

Table 4.1: Parameters of produced biaxial and triaxial preforms

Preform	R[mm]	θ[°]+	LL[mm]	$N_c - N_{cL}$	CF
1	50	30	544.14	144 - 0	0.82
2	50	45	314.159	120 - 0	0.83
3	50	30	544.14	144 - 72	0.93
4	50	30	544.14	96 - 48	0.78
5	50	45	314.16	144 - 72	1
6	50	45	314.16	96 - 48	0.81

It is also possible to control the speed of the horn gear putting the value in the PLC of the machine, but this parameter will influence only the production speed without affecting the cover factor or other geometrical parameters. The Herzog RF 1/144-100 has a range of values for the horn gear speed between 50 and 170 [rpm], but for the production of this preform a value of 50 [rpm] has been used, indeed, as seen before, this value will not affect the geometry of the preform, but it will be only a parameters that controls the production rate, and the choice to set it to the minimum value is linked with the facility of controlling the machine. In Figure 4.3 it is possible to see this production phase.
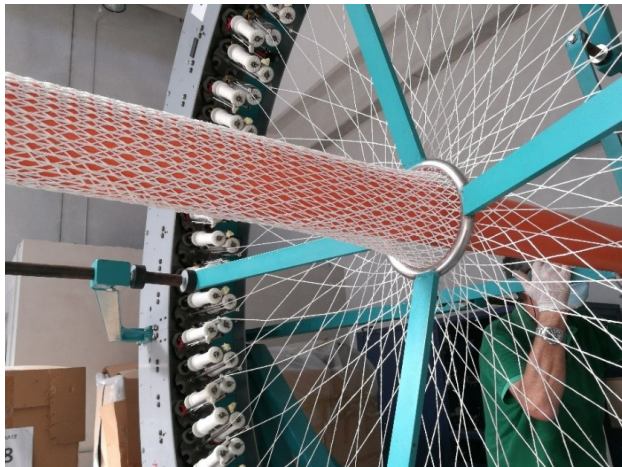
Figure 4.3: Production Process

After this production, the preform is removed from the mandrel and the process is checked. In particular there is a control on:

1. Width of the rotating yarn W_y and width of longitudinal yarn W_{yL}

2. Measure of real value of Cover Factor and comparison with the calculated one

3. Value of Braiding angle

For the first two points, the methodology was explained in the previous chapters, while the braiding angles were checked with a visual inspection, obtaining good results

4.0.1.2 Used Fibres

Nowadays, considering the environmental pushing that the political governments are acting and the increasing interest in the reduction of waste using more eco-friendly materials, it seems necessary to use natural fibres in this kind of work. There are many studies with the aim of finding the best recyclable reinforcement materials [48], and a particular focus is on hemp fibres that result to have some properties similar to the glass fibres [49]. More than this, the production of hemp fibres is one of the greenest under the point of view of the environmental impact and the influence on the territory. Indeed, the values in terms of energy for the production, emissions of harmful agents and more others substances with an influence on the environment are lower with respect to glass fibres ones [50]. Hemp fibres are used in the field of automotive, but because of its hygroscopicity, for now it is impossible to substitute structural parts, so they are used for the interiors. Another field where the hemp is really used is in thermal insulation, and thanks the porosity of this kind of fibres also in soundproofing. For this reason, also in the construction sector the use of hemp is being implemented combined with cement and gypsum [51].

4.0.2 Infusion process of braided preform using RIFT technique

The obtained braided preforms are infused with the RIFT (Resin Infusion under Flexible Tooling) technique to realize composite laminates with hemp fibres. The fibres used are supplied by Fidia s.r.l. which performed also the production of the single yarns. First of all, the preforms were cut in a dimension that can fit in the infusion "chamber" and weighted so to know the percentage of fibres at the end of realization of the specimens. It is necessary to be sure that the braiding angles keep the designed value (4.4)
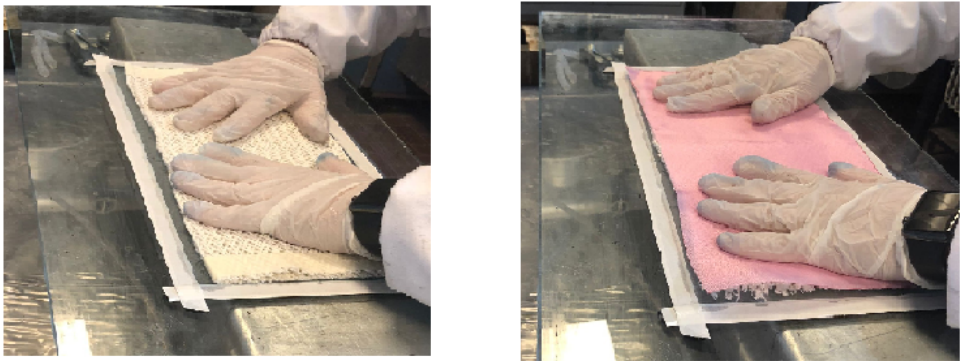
Figure 4.4: Preparation of hemp braided fibers

The used mold is composed by a glass sheet with the same dimension of the fibres. Around the mold was placed a tape to seal the infusion part and a releasing agent was applied so to make easy the removal of the ended laminate. On the fibres was placed the peel-ply that has the function to help the demolding process and to remove the excess resin. A nylon bag was used to close the infusion chamber. The matrix used for the infusion is an epoxy thermoset resin SX10 supplied by Mates. This kind of resin has low viscosity, low toxicity and good mechanical properties [52]. In Table 4.2 can be seen the mechanical properties of the used materials.

Material	E(Mpa)	σ(Mpa)
Epoxy Resin SX10	2700	60
Hemp Yarn	4587	225
Impregnated Hemp Yarn	7823	217

Table 4.2: Mechanical characteristics of used materials

During the infusion process, a difference of pressure (Δp) applied by a pump permits the resin to go through the fibres. In the beginning, the value of Δp is high (0.8 bar), but after a while (when the resin reaches the 3/4 of the length of the preform) the value is decreased (0.6 bar) to obtain small flows of resin inside the single yarn. In 4.5 it is possible to see the infusion process.

Figure 4.5: Infusion process, with particular attention to the flow front

The infusion process is long 30-40 minutes, after which the pump is used to remove the air from the inside, and the laminate is kept for 24 hours to wait the set time of the resin.

Due to the high number of variables during the process, it is easy to find some defects in the final laminate. The common ones are:

- Presence of air bubbles;

- Defects in terms of impregnation of the fibres

- More resin on the edge of the laminate

In 4.6 it is possible to see the final laminate
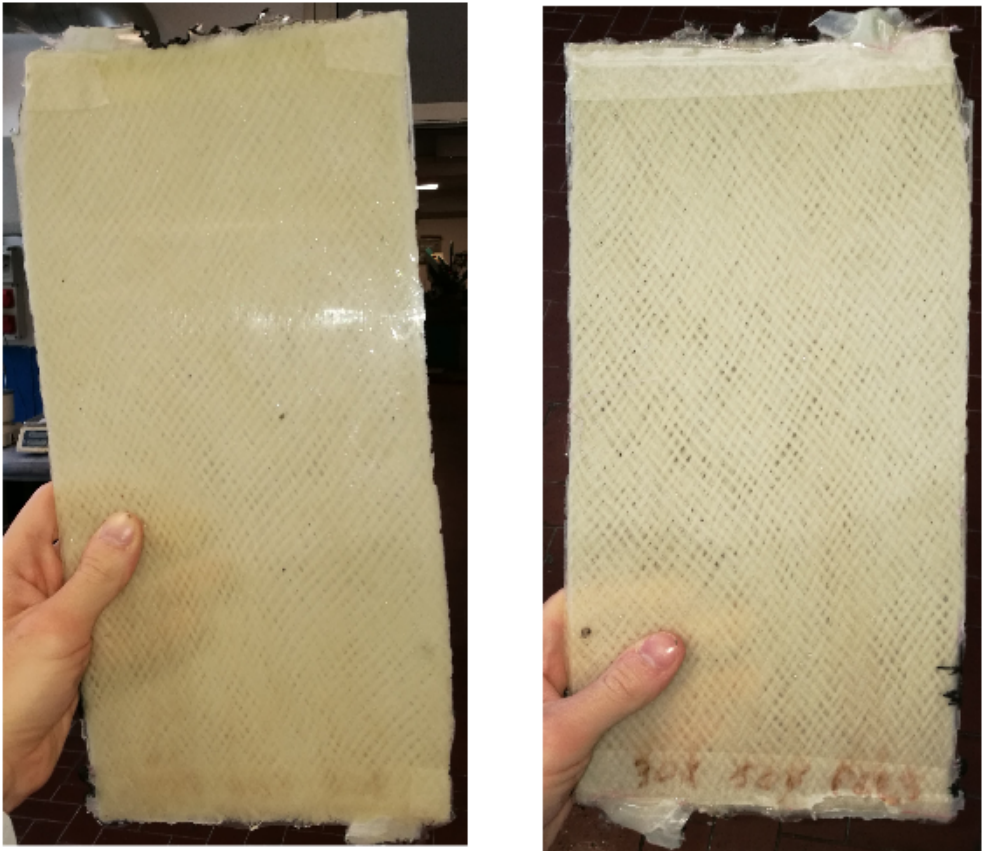
Figure 4.6: Final obtained laminate

4.0.3 Cutting of specimens and mechanical tests

The realized laminates are of 4 typologies and are summarized in the following table (Table 4.3).

Table 4.3: Properties of infused laminate. The CF for the biaxial panel is calculated with the equation 2.6, meanwhile for the triaxial laminates the statistical approach was used

Panel	Reinforce	R[mm]	$\theta[°]$	N_c - N_{cL}	CF
1	Biaxial	50	30	144 - 0	0.78
2	Biaxial	50	45	120 - 0	0.79
3	Triaxial	50	30	96 - 48	0.78
4	Triaxial	50	45	96 - 48	0.81

The results in fibres percentage were calculated obtaining the value of density with an hydrostatics balance measurements. The used instrumentation can be seen in the following Figure (Figure 4.7).

Figure 4.7: Hydrostatic balance to measure the density of the specimens

In Table 4.4 are reported the value of the volume fraction of fibres.

Table 4.4: Value of Density and Fiber Volume Fraction of the laminates

Kind of Specimen	Density $[gr/cm^3]$	Fibres Volume Fraction
50/30	1.1950	30%
50/45	1.1897	31%
TX50/30	1.1522	38%
TX50/45	1.1205	39%

From each one of these laminates, three specimens have been cut by using a diamond circular saw to perform tensile tests, three for flexural tests and four for short beam strength tests. The referred regulations for the dimension of specimens and to perform the tests are:

- ASTM D3039 for tensile tests

- ASTM D790 for flexural tests

- ASTM D2344 for short beam strength tests

A schematic representation of the cut specimens can be seen in
Figure 4.8
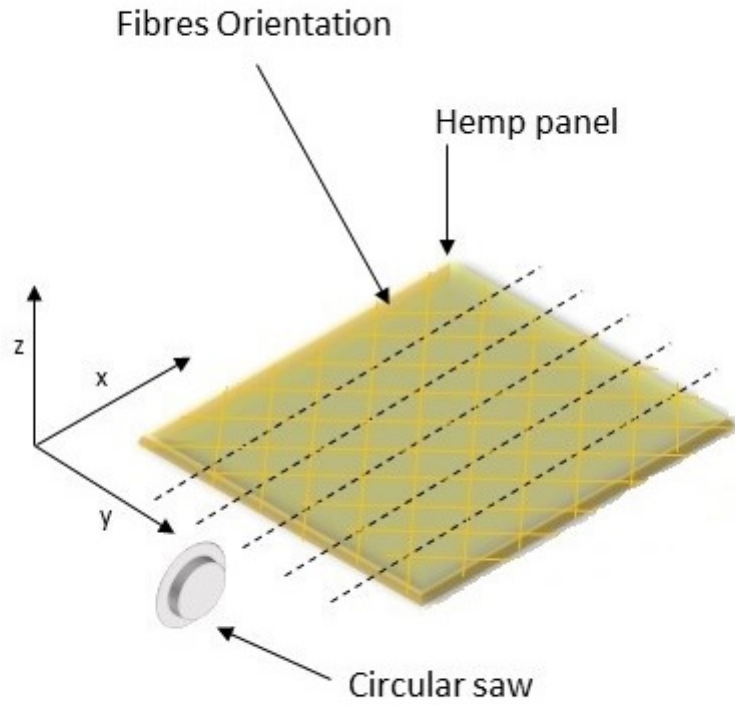
Figure 4.8: A schematic view of the method to cut the specimens

All the mechanical tests were carried out on the MTS Alliance RT/50 (Figure 4.9) using a load cell of 1KN and different types of equipment. The speed of each test is 5[mm/min]

Figure 4.9: Universal testing machine MTS Alliance RT/50

Tensile Tests

For each laminate, three specimens were obtained with a dimension of $200x25x2.5mm$, named TR R/θ-N° for the biaxial and TX TR/θ-N° for the triaxial (obviously, R is the dimension of the mandrel, θ is the braiding angle and N° is the number of the specimen) (Figure 4.10).
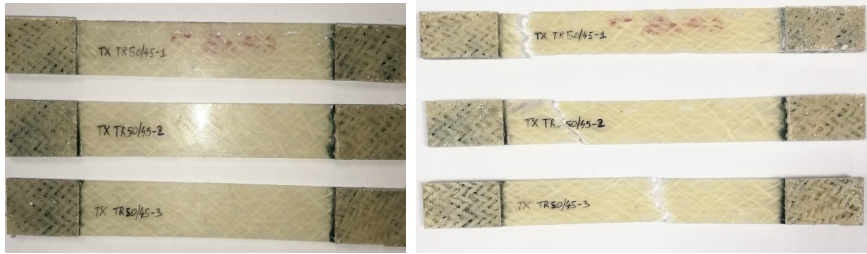
Figure 4.10: Tensile Specimens before and after the test

On the MTS machine jaws were used to grip the specimens and a strain gauge to measure the deformation (Figure 4.11)

Figure 4.11: Equipment for Tensile Tests

The specimens were loaded until the rupture; the acquisition of the load cell and the strain gauge will give the value of the elastic modulus.

$$E_{tr} = \frac{\Delta \sigma}{\Delta \epsilon} \tag{4.1}$$

This equation means that is possible to calculate the Young Modulus as slope of the linear part of the Sigma-Epsilon graph.

Flexural Tests

Also for the flexural tests three specimens were obtained (Figure 4.12).
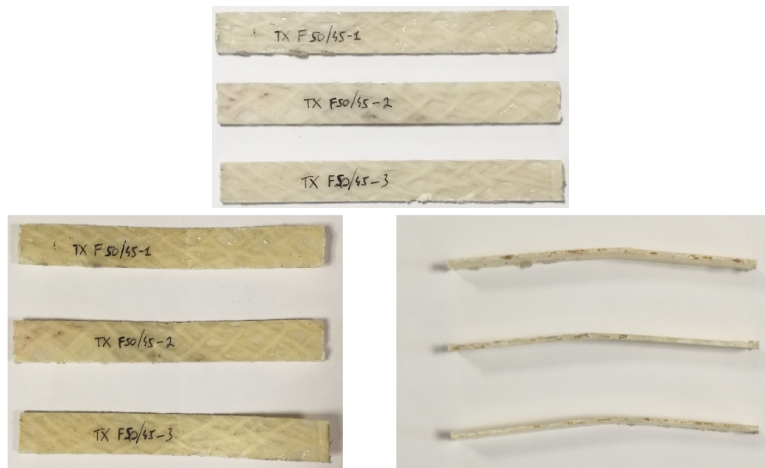
Figure 4.12: Flexural Specimens before and after the test.

They are named F R/θ-N° for biaxial specimens and TX F R/θ-N° for the triaxial ones, and their dimensions will respect the normative $(120x12.5x2.5mm)$.

The equipment used is the one for the 3 points flexural test, with the specimen supported on two points and loaded in the centre, on another point; this is shown in Figure 4.13.

Figure 4.13: Equipment for three points flexural tests

With the following relations it will be possible to calculate the value of maximum tension σ_f and the value of Young Modulus E_f

$$\sigma_f = \frac{3}{2} \frac{P \cdot L}{bd^2} \tag{4.2}$$

$$E_f = \frac{L^3 m}{4bd^3} * 10^-3 \tag{4.3}$$

where

- P[N]: maximum value of load, measured with the load cell

- L[mm]: distance between the support (span). In our case it will be 80mm

- b[mm]: width of the specimen

- d[mm]: the thickness of the specimen

- m: slope of the linear part of the graph Load-Displacement

Short Beam Strength Tests

In this case the number of specimens from each laminate will be four. The biaxial specimens will be named T R/θ-N° and the triaxial ones will be named TX T R/θ-N°. The dimension of the specimens according with the normative results $25x9x3mm$.
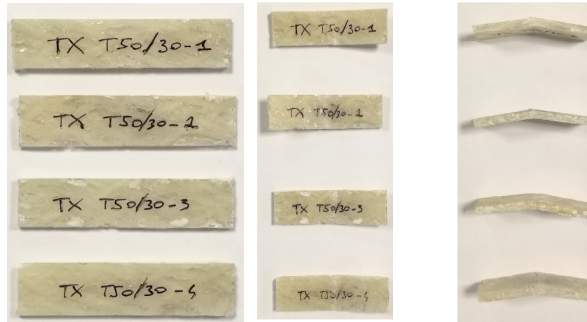
Figure 4.14: Short Beam Strength Specimens before and after the test

The equipment used is similar to the one used in the flexural tests (Figure 4.15), as well as the process.

Figure 4.15: Equipment for Short Beam Strength tests

The thickness and the span of the specimen has to respect the relation

$$1 < \frac{L}{d} < 5$$

In this case, the τ will be higher than σ so to be sure that the rupture is due to the shear stress. Knowing the value of F using the load cell it will be possible to know the value of the τ

$$\tau_{max} = 0.75\frac{F_{max}}{A} \tag{4.4}$$

Chapter 5

Results and discussion of Mechanical Tests: comparison between different preforms

To analyse the influence of braiding angle and of the type of the preform it is necessary to analyse the results of mechanical tests on the laminate. As illustrated above the tested specimens are:

- Laminate obtained from biaxial preform with R=50mm, θ=30° and CF=0.78 (50/30)

- Laminate obtained from biaxial preform with R=50mm, θ=45° and CF=0.79 (50/45)

- Laminate obtained from triaxial preform with R=50mm, θ=30° and CF=0.78 (TX 50/30)

- Laminate obtained from triaxial preform with R=50mm, θ=45° and CF=0.81 (TX 50/45)

In Figure 5.1 it is possible to observe the σ-ϵ curves, obtained from the tensile tests on the laminate.
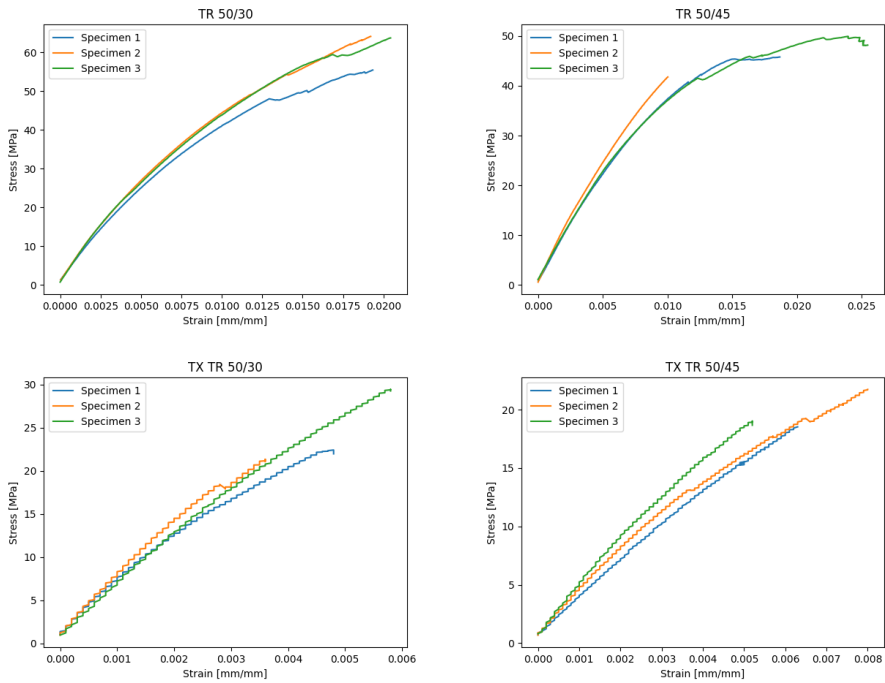
Figure 5.1: Sigma-Epsilon of Tensile Tests for the 4 different types of specimens

The values of $\boldsymbol{\sigma_{tr,max}}$ and $\boldsymbol{E_{tr}}$ for all the specimens analysed, are summarized in Table 5.1

Table 5.1: Results of Tensile tests

Specimen	$\boldsymbol{\sigma_{tr,max}[MPa]}$	$\boldsymbol{E_{tr}[GPa]}$
TR 50/30-1	55.47	5.45
TR 50/30-2	64.07	5.98
TR 50/30-3	63.59	5.87
	Mean: 61.04	**Mean:** 5.77
	St.Dev: 4.83	**St.Dev:** 0.28
TR 50/45-1	45.82	4.76
TR 50/45-2	41.75	5.21
TR 50/45-3	49.83	4.52
	Mean: 45.8	**Mean:** 4.83
	St.Dev: 4.04	**St.Dev:** 0.35
TX TR 50/30-1	43.27	6.75
TX TR 50/30-2	42.1	7.3
TX TR 50/30-3	50.07	6.7
	Mean: 45.15	**Mean:** 6.91
	St.Dev: 4.30	**St.Dev:** 0.33
TX TR 50/45-1	28.18	4.62
TX TR 50/45-2	33.71	5.2
TX TR 50/45-3	33.72	5.5
	Mean: 31.87	**Mean:** 5.11
	St.Dev: 3.19	**St.Dev:** 0.45

From a macromechanical point of view, the preforms with a braiding angle of 30°, respect to loading directions, performs better when subjected to tensile tests compared to the preforms with a 45° braiding angle, as the orientation of the fibres guarantees better properties in the tensile direction.

Indeed, considering separately the biaxial and the triaxial preforms, the theory is confirmed: the preform with θ of 30° has better tensile properties compared to the 45° one (Figure 5.2).
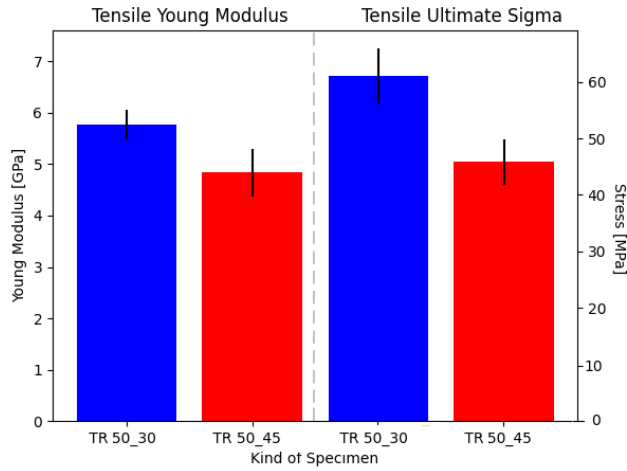
(a)
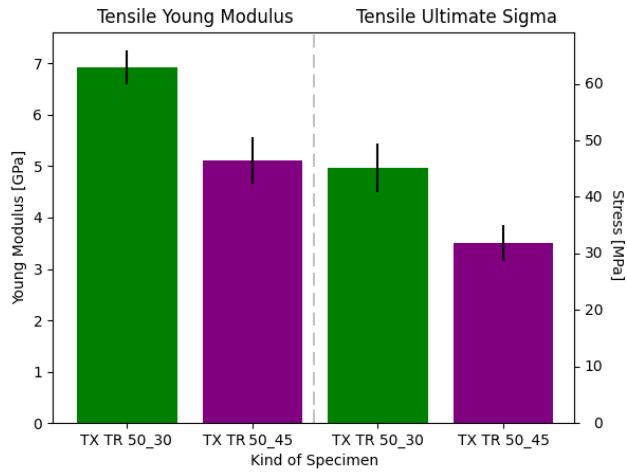
(b)

Figure 5.2: Comparison between Ultimate Sigma and Young Modulus
for tensile tests at different braiding angles. Mean value and standard
deviation. a) is a comparison of biaxial specimens, b) are the triaxial ones.

Considering the comparison between biaxial and triaxial preforms with the same braiding angle, it is expected that the preforms with longitudinal fibres will have better characteristics. In Figure 5.3 it is clear that this is true as concerns the value of the Young Modulus; however, as evident from the graphs, the value of the ultimate tensile strength is lower for the triaxial preforms.
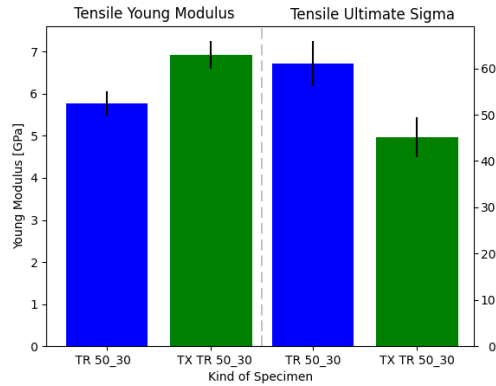
(a)
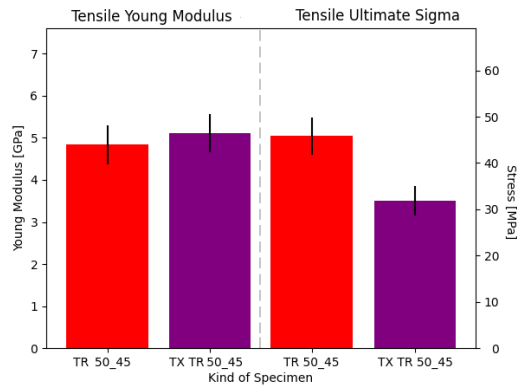
(b)

Figure 5.3: Comparison between Ultimate Sigma and Young Modulus subjected to tensile tests for biaxial and triaxial specimens. Mean value and standard deviation. a) is a comparison of 30° specimens, b) is referred to 45° specimens.

The reason could be ascribed to the difficulties in the tensioning of hemp yarns during the production phase, as crimping effects take place with consequent presence of voids during the impregnation [53, 54, 55]. Moreover, it is possible to obtain an esteem of the percentage of voids inside the specimen analyzing the cross-section images (obtained by means of a Confocal Lext Olympus OLS 5000 microscope) converted in binary through MATLAB software (Figure 5.4, Figure 5.5). For each typology of braided preform 2 specimens were analyzed and as result, the Biaxial specimens will have a percentage of voids of 6.16% and 7.91%, respectively for braiding angle of 30 degrees and 45 degrees; the Triaxial one will have a percentage of voids of 11.47% and 16.26% with a braiding angle respectively of 30 and 45 degrees. This confirms the lower value of the ultimate stress of the triaxial specimens.
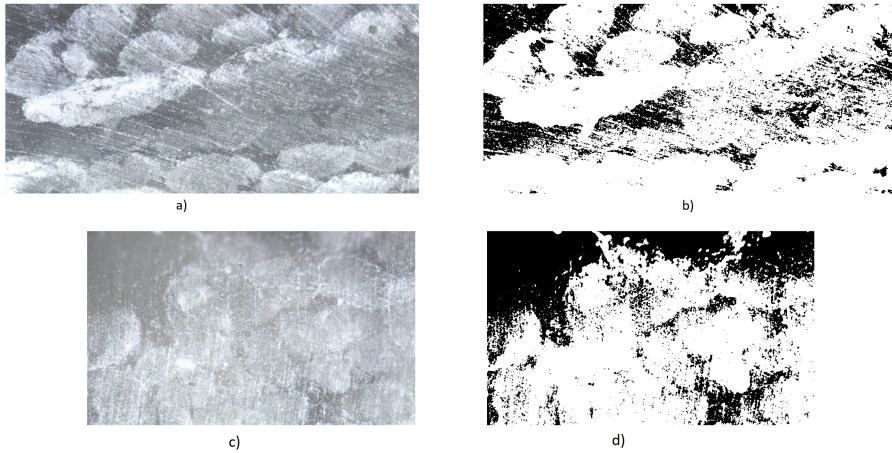
Figure 5.4: Presence of voids for the specimens R50/30 biaxial and
triaxial: a) and b) correspond to Biaxial, c) and d) correspond to Triaxial
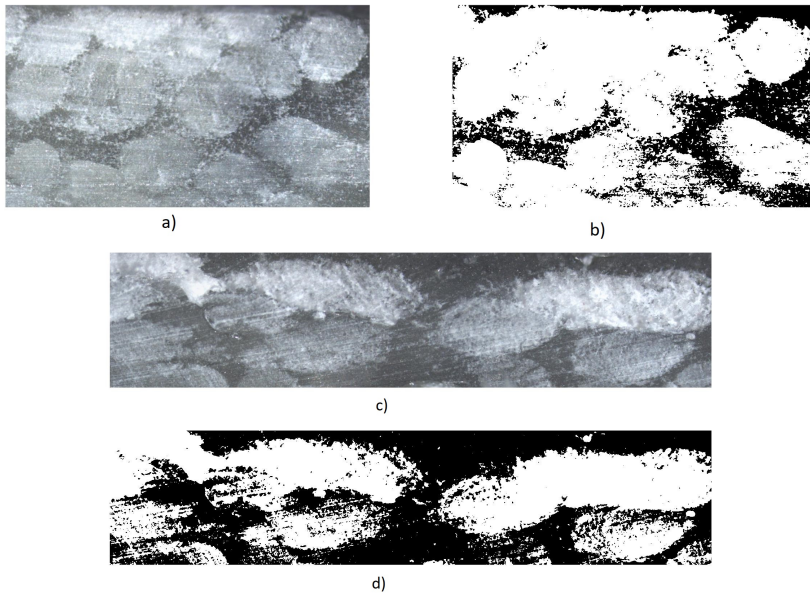
Figure 5.5: Presence of voids for the specimens R50/45 biaxial and
triaxial: a) and b) correspond to Biaxial, c) and d) correspond to Triaxial

The three points flexural test results are shown in Figure 5.6, where
it is possible to see the Load-Displacement curves for each typology of
specimens and the corresponding Stress-Strain curves (Figure 5.7).
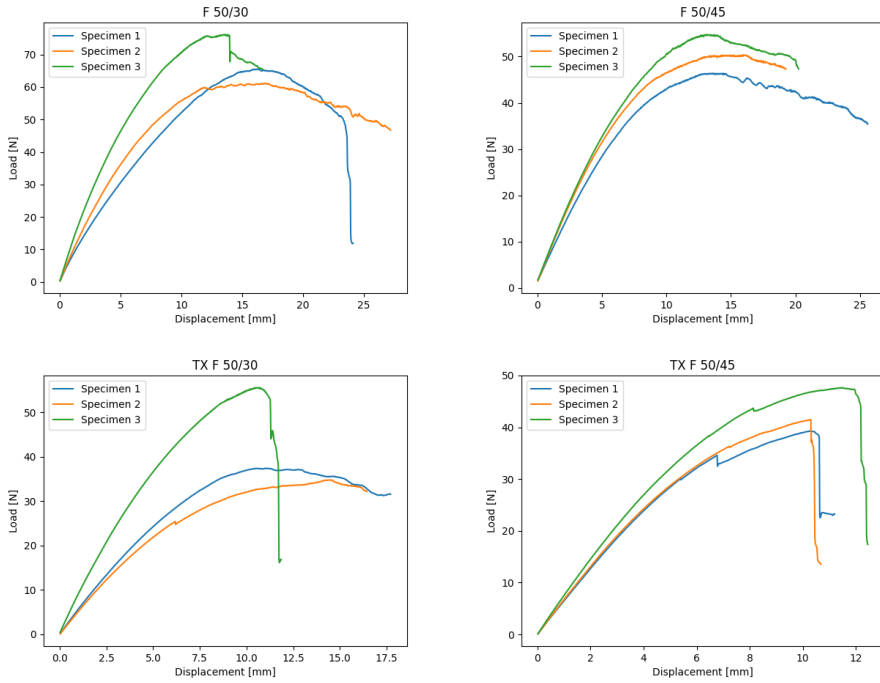
Figure 5.6: Load-Displacement of three points flexural Tests for the 4
different types of specimens
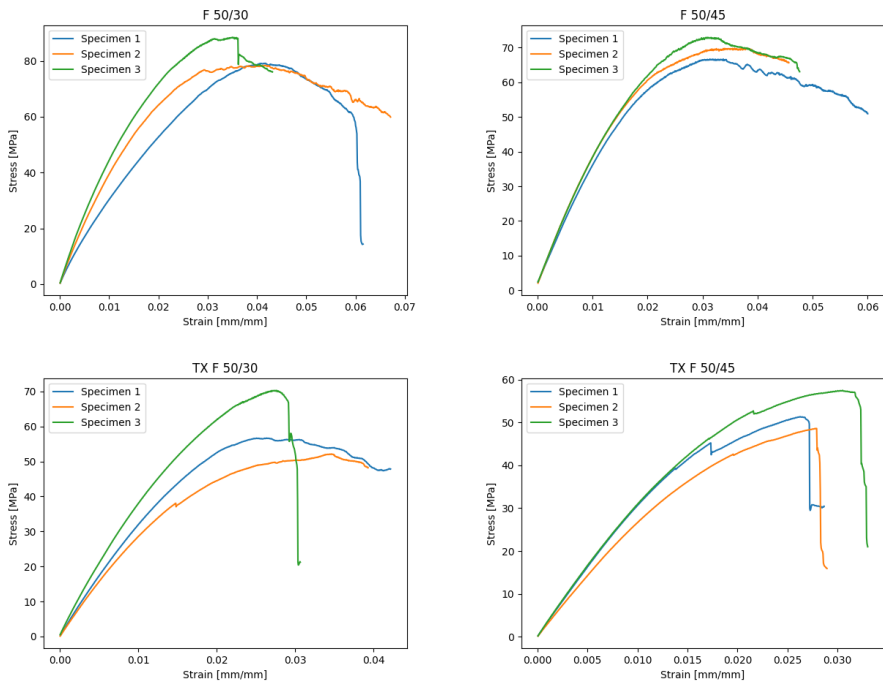
Figure 5.7: Stress-Strain of three points flexural Tests for the 4 different
types of specimens

The values of the Young Modulus and Tension of Rupture of the above mentioned specimens are summarized in Table 5.2

Table 5.2: Results of three points flexural tests

Specimen	$\sigma_{f,max}[MPa]$	$E_f[GPa]$
F 50/30-1	79.2	3.52
F 50/30-2	78.45	4.6
F 50/30-3	88.47	5.32
	Mean: 82.04	**Mean:** 4.48
	St.Dev: 5.58	**St.Dev:** 0.90
F 50/45-1	66.7	3.67
F 50/45-2	70	4.17
F 50/45-3	72.95	4.02
	Mean: 69.88	**Mean:** 3.95
	St.Dev: 3.13	**St.Dev:** 0.26
TX F 50/30-1	69.73	3.54
TX F 50/30-2	64.65	3.30
TX F 50/30-3	75.5	4.42
	Mean: 69.96	**Mean:** 3.75
	St.Dev: 5.42	**St.Dev:** 0.59
TX F 50/45-1	51.36	3.27
TX F 50/45-2	48.63	2.88
TX F 50/45-3	57.52	3.36
	Mean: 52.50	**Mean:** 3.17
	St.Dev: 4.55	**St.Dev:** 0.25

In this case the situation is different. Indeed, the trend of the results is unexpected, and this can be seen in Figure 5.8 and in Figure 5.9. Besides the presence of the voids that influence all the mechanical properties of the specimens, it has to be considered that the samples are composed by two laminates and, as said, the cover factor is different from the unit value. Consequently, the width of the tested specimens could not be enough to consider the fibres inside; this means that other tests are to be performed, out of normative, to find the best width of the specimens that allows to study the flexural and the short beam behaviour of this kind of laminates.
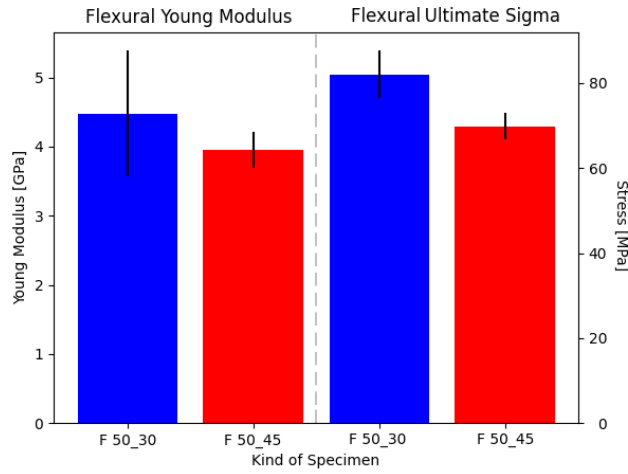
(a)
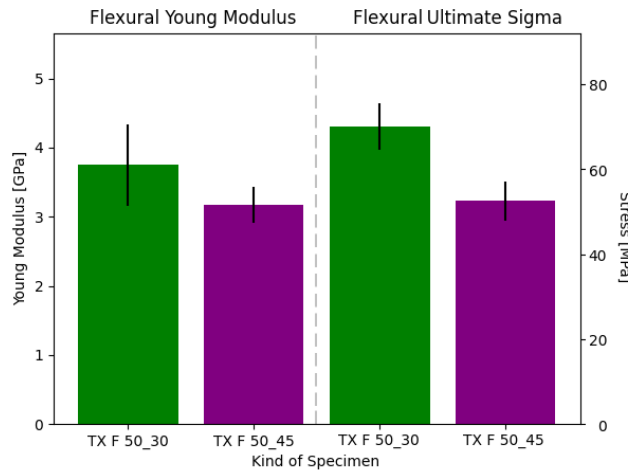
(b)

Figure 5.8: Comparison between Ultimate Sigma and Young Modulus for 3 Points Flexural Tests at different braiding angles. Mean Value and Standard Deviation. a) is a comparison of biaxial specimens, b) are the triaxial ones.
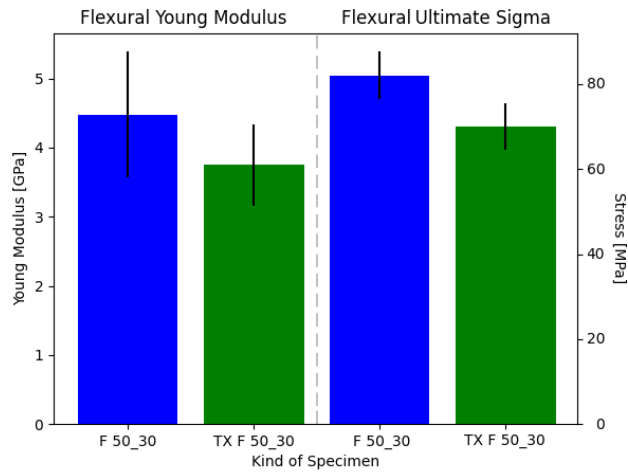
(a)
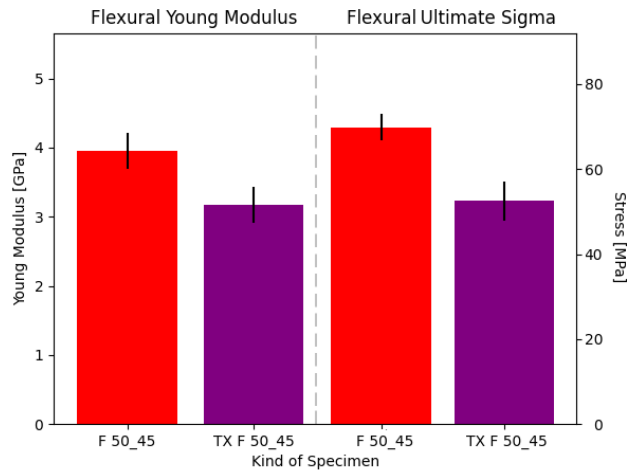
(b)

Figure 5.9: Comparison between Ultimate Sigma and Young Modulus
subjected to 3 Points Flexural Tests for biaxial and triaxial specimens.
Mean Value and Standard Deviation. a) is a comparison of 30° specimens,
b) is referred to 45° specimens.

In addition to this, for the short beam tests, the crimp effect of longitudinal fibres could be predominant so to influence the value of ultimate stress resistance τ for the TX TR specimens. Indeed, implementing the equation 4.4 it is possible to assess the values of τ_{max} reported in Table 5.3 and in Figure 5.10.
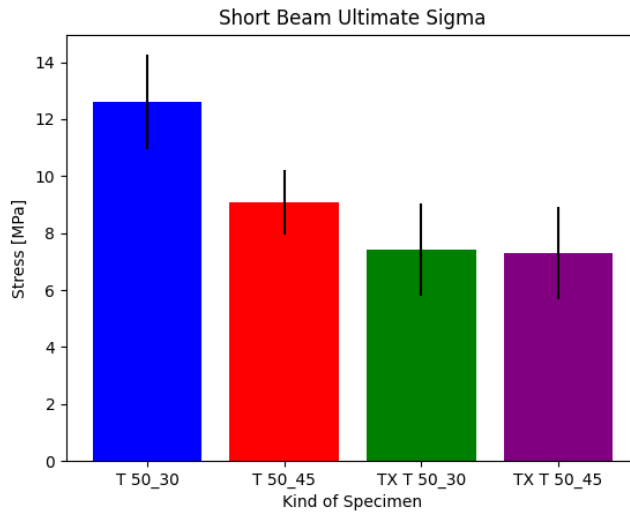
Figure 5.10: Rupture and Young Modulus for short beam tests for each typology of specimens. Mean value and standard deviation

Table 5.3: Results of short beam strength test

Biaxial Specimen	$\tau_{max}[MPa]$	Triaxial Specimen	$\tau_{max}[MPa]$
T 50/30-1	12	TX T 50/30-1	5.28
T 50/30-2	14.2	TX T 50/30-2	7.08
T 50/30-3	13.66	TX T 50/30-3	8.96
T 50/30-4	10.55	TX T 50/30-4	8.30
Mean: 12.56		**Mean:** 7.40	
St. Dev: 1.60		**St. Dev:** 1.62	
T 50/45-1	8.85	TX T 50/45-1	8.95
T 50/45-2	10.35	TX T 50/45-2	7.84
T 50/45-3	7.64	TX T 50/45-3	5.09
T 50/45-4	9.49	TX T 50/45-4	7.30
Mean: 9.07		**Mean:** 7.29	
St. Dev: 1.14		**St. Dev:** 1.62	

As said, the tensioning of fibres during the production could be an explanation of this kind of behaviour. Indeed, the value of Cover Factor for all the preforms is approximately 0.78; this means that the fibres are really close to each others and therefore, after the removal of the preform from the mandrel, they should remain stuck in the chosen position. However, the tensioning of the fibres, due to the small rigidity of the spring, is not enough to avoid the crimping problem when the hemp fibres are used, as they require a considerable tensioning during the braiding production phase due to their high elasticity.

Conclusions

This work permits to describe an analytical process to forecast the exact value of cover factor obtained by realizing biaxial and triaxial preforms. In this way, it will be possible to handle in a better way the production parameters on the braiding machine, obtaining an error in the estimation of cover factor that will be less than 5%.

This allowed to obtain biaxial and triaxial preforms, made of hemp fibres, with the same value of cover factor and consequently a comparable value of volumetric fiber fraction. With this methodology, it will be possible to compare the two different types of reinforcements by performing mechanical tests to describe the mechanical behaviour of the laminates obtained with the braiding process.

In terms of Elastic Modulus, it will be clear that the presence of longitudinal fibres will increase the value of the modulus giving to the triaxial braided preform a higher rigidity. On the contrary, it turned out that for the triaxial preforms there is an effect due to the overlap of the fibres that brings to a lower value of ultimate strength. This effect, called crimping, affects the value of tensile strength of 26% for the 30° laminates and of 30% for 45° laminates. In terms of flexural strength, the reduction of ultimate values will be respectively of 15% and 24%. For the short beam tests, instead, the variation will be 30%. A comparison of this data with the fiber volume fraction (the triaxial specimens have 10% more fibres, in volume, than the biaxial ones) shows that the crimping effect will be really consistent and it will be necessary to increase the tensioning of the fibres during the production to avoid the reduction of these values.

Actually, in the description of the braiding machine, it has been underlined that to realize preforms without defects it is necessary to use carriers with springs capable of guaranteeing the right tensioning and alignment of the yarns on the mandrel.

However, the used machine was developed for materials with high elas-

tic modulus such as glass and carbon fibres; for this reason, to optimize the braiding process with natural fibres, it is necessary to change the springs and to design them with higher rigidity, in order to give the right tensioning to fibres with a lower elasticity.

In addition, the higher percentage of voids (almost twice) contributes to the decreasing of the ultimate strength properties in the laminate with longitudinal fibers, but also this effect could be linked with the crimping phenomenon that doesn't allow the resin to flow homogeneously.

Further deeper investigations will be necessary to design new springs and to solve the crimping problem, so that it will be possible to use a braiding process with natural fibres to obtain laminates without voids and with an higher ultimate resistance.

Bibliography

[1] J P Carey. "1 - Introduction to braided composites". In: *Handbook of Advances in Braided Composite Materials*. Ed. by Jason P Carey. Woodhead Publishing, 2017, pp. 1–21. ISBN: 978-0-08-100369-5. DOI: https://doi.org/10.1016/B978-0-08-100369-5.00001-5. URL: http://www.sciencedirect.com/science/article/pii/B9780081003695000015.

[2] David Branscomb, David Beale, and Royall Broughton. "New Directions in Braiding". In: *Journal of Engineered Fibers and Fabrics* 8.2 (June 2013), p. 155892501300800. ISSN: 1558-9250. DOI: 10.1177/155892501300800202. URL: http://www.eejournal.com/archives/articles/20110301-zynq%20http://journals.sagepub.com/doi/10.1177/155892501300800202.

[3] A A Head, F K Ko, and C M Pastore. *Handbook of Industrial Braiding*. Atkins and Pearce, 1990. URL: https://books.google.it/books?id=TmFIQwAACAAJ.

[4] Cagri Ayranci and Jason Carey. "2D braided composites: A review for stiffness critical applications". In: *Composite Structures* 85.1 (2008), pp. 43–58. ISSN: 02638223. DOI: 10.1016/j.compstruct.2007.10.004.

[5] "Woodhead Publishing Series in Textiles". In: *Advances in Braiding Technology*. Ed. by Yordan Kyosev. Woodhead Publishing Series in Textiles. Woodhead Publishing, 2016, pp. xv–xxii. ISBN: 978-0-08-100926-0. DOI: https://doi.org/10.1016/B978-0-

08-100407-4.09002-5. URL: http://www.sciencedirect.com/science/article/pii/B9780081004074090025.

[6] Dan Adams. "Effects of yarn crimping on braided composite design allowables". In: (1996).

[7] C. C. Poe, H. B. Dexter, and I. S. Raju. "Review of the NASA textile composites research". In: *Collection of Technical Papers - AIAA/ASME/ASCE/AHS/ASC Structures, Structural Dynamics and Materials Conference* 2 (1997), pp. 1126–1138. ISSN: 02734508. DOI: 10.2514/6.1997-1321.

[8] Michael Bannister. "Challenges for composites into the next millennium - A reinforcement perspective". In: *Composites - Part A: Applied Science and Manufacturing* 32.7 (2001), pp. 901–910. ISSN: 1359835X. DOI: 10.1016/S1359-835X(01)00008-2.

[9] H Benson Dexter. "Development of Textile Reinforced Composites for Aircraft Structures". In: *4th International Symposium for Textile Composites* (1998), pp. 1–8.

[10] Karin Birkefeld et al. "Characterization of Biaxial and Triaxial Braids: Fiber Architecture and Mechanical Properties". In: *Applied Composite Materials* 19.3-4 (June 2012), pp. 259–273. ISSN: 0929-189X. DOI: 10.1007/s10443-011-9190-2. URL: http://link.springer.com/10.1007/s10443-011-9190-2.

[11] P. Potluri et al. "Geometrical modelling and control of a triaxial braiding machine for producing 3D preforms". In: *Composites Part A: Applied Science and Manufacturing* 34.6 SPEC. (2003), pp. 481–492. ISSN: 1359835X. DOI: 10.1016/S1359-835X(03)00061-7.

[12] M Munro and A Fahim. "A Comparison of Helical Filament Winding and 2D Braiding of Fiber Reinforced Polymeric Components". In: *Materials and Manufacturing Processes* 10.1 (1995),

pp. 37–46. DOI: 10.1080/10426919508936925. URL: https://doi.org/10.1080/10426919508936925.

[13] A Pickett et al. "Comparison of analytical and finite element simulation of 2D braiding". In: *Plastics, Rubber and Composites* 38.9-10 (2009), pp. 387–395. DOI: 10.1179/146580109X12540995045769. URL: https://doi.org/10.1179/146580109X12540995045769.

[14] Anubhav Singh et al. "The effect of braid angle on the flexural performance of structural braided thermoplastic composite beams". In: *Composite Structures* 261 (Apr. 2021), p. 113314. ISSN: 02638223. DOI: 10.1016/j.compstruct.2020.113314. URL: https://linkinghub.elsevier.com/retrieve/pii/S0263822320332402.

[15] Nesrin Sahbaz Karaduman et al. "Textile Reinforced Structural Composites for Advanced Applications". In: *Textiles for Advanced Applications*. InTech, Sept. 2017. DOI: 10.5772/intechopen.68245. URL: http://www.intechopen.com/books/textiles-for-advanced-applications/textile-reinforced-structural-composites-for-advanced-applications.

[16] D Brunnschweiler. "BRAIDS AND BRAIDING". In: *Journal of the Textile Institute Proceedings* 44.9 (1953), P666–P686. DOI: 10.1080/19447015308687874. URL: https://doi.org/10.1080/19447015308687874.

[17] Garrett W. Melenka and Jason P. Carey. "Braid CAM: Braided composite analytical model". In: *SoftwareX* 7 (2018), pp. 23–27. ISSN: 23527110. DOI: 10.1016/j.softx.2017.12.004. URL: https://doi.org/10.1016/j.softx.2017.12.004.

[18] Conference Paper et al. "Effect of Preform Architecture on the Mechanical and Fatigue Behavior of Braided Composites ..." In: May 2016 (2009).

[19]   John E. Masters and Peter G. Ifju. "A phenomenological study of triaxially braided textile composites loaded in tension". In: *Composites Science and Technology* 56.3 (1996), pp. 347–358. ISSN: 02663538. DOI: `10.1016/0266-3538(95)00106-9`.

[20]   G W Melenka et al. "3 - Manufacturing processes for braided composite materials". In: *Handbook of Advances in Braided Composite Materials*. Ed. by Jason P Carey. Woodhead Publishing, 2017, pp. 47–153. ISBN: 978-0-08-100369-5. DOI: `https://doi.org/10.1016/B978-0-08-100369-5.00003-9`. URL: `http://www.sciencedirect.com/science/article/pii/B9780081003695000039`.

[21]   T Uozumi, A Kito, and T Yamamoto. "CFRP using braided preforms/RTM process for aircraft applications". In: *Advanced Composite Materials* 14.4 (2005), pp. 365–383. DOI: `10.1163/156855105774470366`. URL: `https://doi.org/10.1163/1568551057744703`

[22]   R. T. Hans and Hinterhoelzl. "A NUMERICAL APPROACH MODELING THE BRAIDING PROCESS FOR ARBITRARY MANDREL SHAPES TO CALCULATE PREFORM PROPERTIES". In: *20th International Conference on Composite Materials Copenhagen* (2015).

[23]   Makiko Tada et al. "Structure and machine braiding procedure of coupled square braids with various cross sections". In: *Composites - Part A: Applied Science and Manufacturing* 32.10 (2001), pp. 1485–1489. ISSN: 1359835X. DOI: `10.1016/S1359-835X(01)00047-1`.

[24]   A. C. Long. "Process modelling for liquid moulding of braided preforms". In: *Composites - Part A: Applied Science and Manufacturing* 32.7 (2001), pp. 941–953. ISSN: 1359835X. DOI: `10.1016/S1359-835X(00)00153-6`.

[25]   J. F.A. Kessels and R. Akkerman. "Prediction of the yarn tra-
       jectories on complex braided preforms". In: *Composites Part A:*
       Applied Science and Manufacturing 33.8 (2002), pp. 1073–1081.
       ISSN: 1359835X. DOI: 10.1016/S1359-835X(02)00075-1.

[26]   Guangli Ma, David J. Branscomb, and David G. Beale. "Model-
       ing of the tensioning system on a braiding machine carrier". In:
       Mechanism and Machine Theory 47.1 (2012), pp. 46–61. ISSN:
       0094114X. DOI: 10.1016/j.mechmachtheory.2011.08.008.
       URL: http://dx.doi.org/10.1016/j.mechmachtheory.2011.
       08.008.

[27]   G w. Du and P Popper. "Analysis of a Circular Braiding Process
       for Complex Shapes". In: *The Journal of The Textile Institute*
       85.3 (1994), pp. 316–337. DOI: 10.1080/00405009408631277.
       URL: https://doi.org/10.1080/00405009408631277.

[28]   Philippe Monnot, Jonathan Lévesque, and Louis Laberge Lebel.
       "Automated braiding of a complex aircraft fuselage frame us-
       ing a non-circular braiding model". In: *Composites Part A: Ap-*
       plied Science and Manufacturing 102 (2017), pp. 48–63. ISSN:
       1359835X. DOI: 10.1016/j.compositesa.2017.07.011. URL:
       https://doi.org/10.1016/j.compositesa.2017.07.011.

[29]   F. Heieck et al. "Influence of the cover factor of 2D biaxial and
       triaxial braided carbon composites on their in-plane mechanical
       properties". In: *Composite Structures* 163 (2017), pp. 114–122.
       ISSN: 02638223. DOI: 10.1016/j.compstruct.2016.12.025.
       URL: http://dx.doi.org/10.1016/j.compstruct.2016.12.
       025.

[30]   "6 - Braiding machine components". In: *Braiding Technology*
       for Textiles. Ed. by Y Kyosev. Woodhead Publishing Series in
       Textiles. Woodhead Publishing, 2015, pp. 115–151. ISBN: 978-0-
       85709-135-2. DOI: https://doi.org/10.1533/9780857099211.

2 . 115. URL: `http : / / www . sciencedirect . com / science / article/pii/B9780857091352500064`.

[31] Donghang Liu, Meijing Tang, and Jianhua Yan. "Comparative study of the tensile properties of 2D and UD over-braided multilayer composites". In: *Composites Science and Technology* 210 (July 2021), p. 108817. ISSN: 02663538. DOI: `10.1016/j.compscitech. 2021 . 108817`. URL: `https : / / linkinghub . elsevier . com / retrieve/pii/S0266353821001731`.

[32] Georgios Balokas et al. "Stochastic modeling techniques for textile yarn distortion and waviness with 1D random fields". In: *Composites Part A: Applied Science and Manufacturing* 127 (Dec. 2019), p. 105639. ISSN: 1359835X. DOI: `10.1016/j.compositesa. 2019 . 105639`. URL: `https : / / linkinghub . elsevier . com / retrieve/pii/S1359835X19303884`.

[33] R.F.J. McCarthy, G.H. Haines, and R.A. Newley. "Polymer composite applications to aerospace equipment". In: *Composites Manufacturing* 5.2 (June 1994), pp. 83–93. ISSN: 09567143. DOI: `10. 1016/0956 - 7143(94)90059 - 0`. URL: `https : // linkinghub . elsevier.com/retrieve/pii/0956714394900590`.

[34] Chaojing Li et al. "Modeling of braiding parameter impact on pore size and porosity in a tubular braiding fabric". In: *e-Polymers* 17.3 (May 2017), pp. 221–226. ISSN: 1618-7229. DOI: `10.1515/ epoly-2016-0060`. URL: `https://www.degruyter.com/document/ doi/10.1515/epoly-2016-0060/html`.

[35] Shu Ching Quek et al. "Analysis of 2D triaxial flat braided textile composites". In: *International Journal of Mechanical Sciences* 45.6-7 (2003), pp. 1077–1096. ISSN: 00207403. DOI: `10.1016/j. ijmecsci.2003.09.003`.

[36] E. E. Swery et al. "Complete simulation process chain for the manufacturing of braided composite parts". In: *Composites Part A: Applied Science and Manufacturing* 102 (2017), pp. 378–390.

ISSN: 1359835X. DOI: 10.1016/j.compositesa.2017.08.011.
URL: https://doi.org/10.1016/j.compositesa.2017.08.011.

[37] D Beale and Ross Hall. "Analysis of Circular Braiding Process , Part 1 : Theoretical Investigation of Kinematics of the Circular Braiding Process". In: *Journal of Manufacturing Science and Engineering* 121.August (1999), pp. 345–350. ISSN: 10871357. DOI: 10.1115/1.2832687.

[38] J. H. Van Ravenhorst and R. Akkerman. "Circular braiding take-up speed generation using inverse kinematics". In: *Composites Part A: Applied Science and Manufacturing* 64 (2014), pp. 147–158. ISSN: 1359835X. DOI: 10.1016/j.compositesa.2014.04.020. URL: http://dx.doi.org/10.1016/j.compositesa.2014.04.020.

[39] G. W. Melenka et al. *Advances in 2-D and 3-D braided composite material modeling.* 2016, pp. 321–363. ISBN: 9780081003770. DOI: 10.1016/B978-0-08-100369-5.00009-X.

[40] Joon Hyung Byun. "The analytical characterization of 2-D braided textile composites". In: *Composites Science and Technology* 60.5 (2000), pp. 705–716. ISSN: 02663538. DOI: 10.1016/S0266-3538(99)00173-6. URL: http://dx.doi.org/10.1016/S0266-3538(99)00173-6.

[41] Garrett W Melenka and Jason P Carey. "Development of a generalized analytical model for tubular braided-architecture composites". In: *Journal of Composite Materials* 51.28 (2017), pp. 3861–3875. DOI: 10.1177/0021998317695421. URL: https://doi.org/10.1177/0021998317695421.

[42] Garrett W Melenka and Jason P Carey. "Experimental analysis of diamond and regular tubular braided composites using three-dimensional digital image correlation". In: *Journal of Com-*

posite Materials 51.28 (2017), pp. 3887–3907. DOI: 10.1177/0021998317695418. URL: https://doi.org/10.1177/0021998317695418.

[43]   Amit Rawal, Prasad Potluri, and Colin Steele. "Geometrical Modeling of the Yarn Paths in Three-dimensional Braided Structures". In: *Journal of Industrial Textiles* 35.2 (Oct. 2005), pp. 115–135. ISSN: 1528-0837. DOI: 10.1177/1528083705057574. URL: http://journals.sagepub.com/doi/10.1177/1528083705057574.

[44]   W. Michaeli, U. Rosenbaum, and M. Jehrke. "Processing strategy for braiding of complex-shaped parts based on a mathematical process description". In: *Composites Manufacturing* 1.4 (Dec. 1990), pp. 243–251. ISSN: 09567143. DOI: 10.1016/0956-7143(90)90047-Z. URL: https://linkinghub.elsevier.com/retrieve/pii/095671439090047Z.

[45]   Yan Tao Gao, Frank K. Ko, and Hong Hu. "Integrated design for manufacturing of braided preforms for advanced composites part I: 2D braiding". In: *Applied Composite Materials* 20.6 (2013), pp. 1007–1023. ISSN: 0929189X. DOI: 10.1007/s10443-012-9303-6.

[46]   "13 - Computer assisted design (CAD) software for the design of braided structures". In: *Braiding Technology for Textiles*. Ed. by Y Kyosev. Woodhead Publishing Series in Textiles. Woodhead Publishing, 2015, pp. 315–336. ISBN: 978-0-85709-135-2. DOI: https://doi.org/10.1533/9780857099211.4.315.

[47]   J.H. van Ravenhorst. "Design tools for circular overbraiding of complex mandrels". PhD thesis. Enschede, The Netherlands: University of Twente, Sept. 2018. ISBN: 9789036545860. DOI: 10.3990/1.9789036545860. URL: http://purl.org/utwente/doi/10.3990/1.9789036545860.

[48]   James Thomason, Liu Yang, and Fiona Gentles. "Characterisation of the Anisotropic Thermoelastic Properties of Natural Fibres for Composite Reinforcement". In: *Fibers* 5.4 (Sept. 2017),

p. 36. ISSN: 2079-6439. DOI: 10.3390/fib5040036. URL: `https://www.mdpi.com/2079-6439/5/4/36`.

[49] H.N. Dhakal and Z. Zhang. "The use of hemp fibres as reinforcements in composites". In: *Biofiber Reinforcements in Composite Materials*. Elsevier, 2015, pp. 86–103. DOI: `10.1533/9781782421276.1.86`. URL: `https://linkinghub.elsevier.com/retrieve/pii/B9781782421221500034`.

[50] Hayo M.G.van der Werf. "Life Cycle Analysis of field production of fibre hemp, the effect of production practices on environmental impacts". In: *Euphytica* 140 (2004), pp. 13–23. URL: `http://www.ingentaconnect.com/content/klu/euph/2004/00000140/F0020001/00004750%7B%5C%%7D5Cnjsessionid=o5t0ck573oeo.alice`.

[51] Luca Boccarusso et al. "Production of hemp-gypsum composites with enhanced flexural and impact resistance". In: *Construction and Building Materials* 260 (Nov. 2020), p. 120476. ISSN: 09500618. DOI: `10.1016/j.conbuildmat.2020.120476`. URL: `https://linkinghub.elsevier.com/retrieve/pii/S0950061820324818`.

[52] Mates Composite. *Thermoset Resin SX10*. URL: `https://www.mates.it/it/prodotti/resine-adesivi-chimici/resine/epossidica-r/liquide/`.

[53] Nicola Tessitore and Aniello Riccio. "A novel FEM model for biaxial non-crimp fabric composite materials under tension". In: *Computers & Structures* 84.19-20 (July 2006), pp. 1200–1207. ISSN: 00457949. DOI: `10.1016/j.compstruc.2006.01.024`. URL: `https://linkinghub.elsevier.com/retrieve/pii/S0045794906001052`.

[54] Daniel O. Adams Alison C. West. "Axial Yarn Crimping Effects in Braided Composite Materials". In: *Journal of Composite Materials* 33 (1998), pp. 5/1999.

[55] Mengru Li et al. "Effect of Fabric Architecture on Tensile Behaviour of the High-Molecular-Weight Polyethylene 3-Dimensional Interlock Composite Reinforcements". In: *Polymers* 12.5 (May 2020), p. 1045. ISSN: 2073-4360. DOI: 10.3390/polym12051045. URL: https://www.mdpi.com/2073-4360/12/5/1045.